EURODYN 2020

XI International Conference on Structural Dynamics

PROCEEDINGS

Volume II

M. Papadrakakis, M. Fragiadakis, C. Papadimitriou (Eds.)

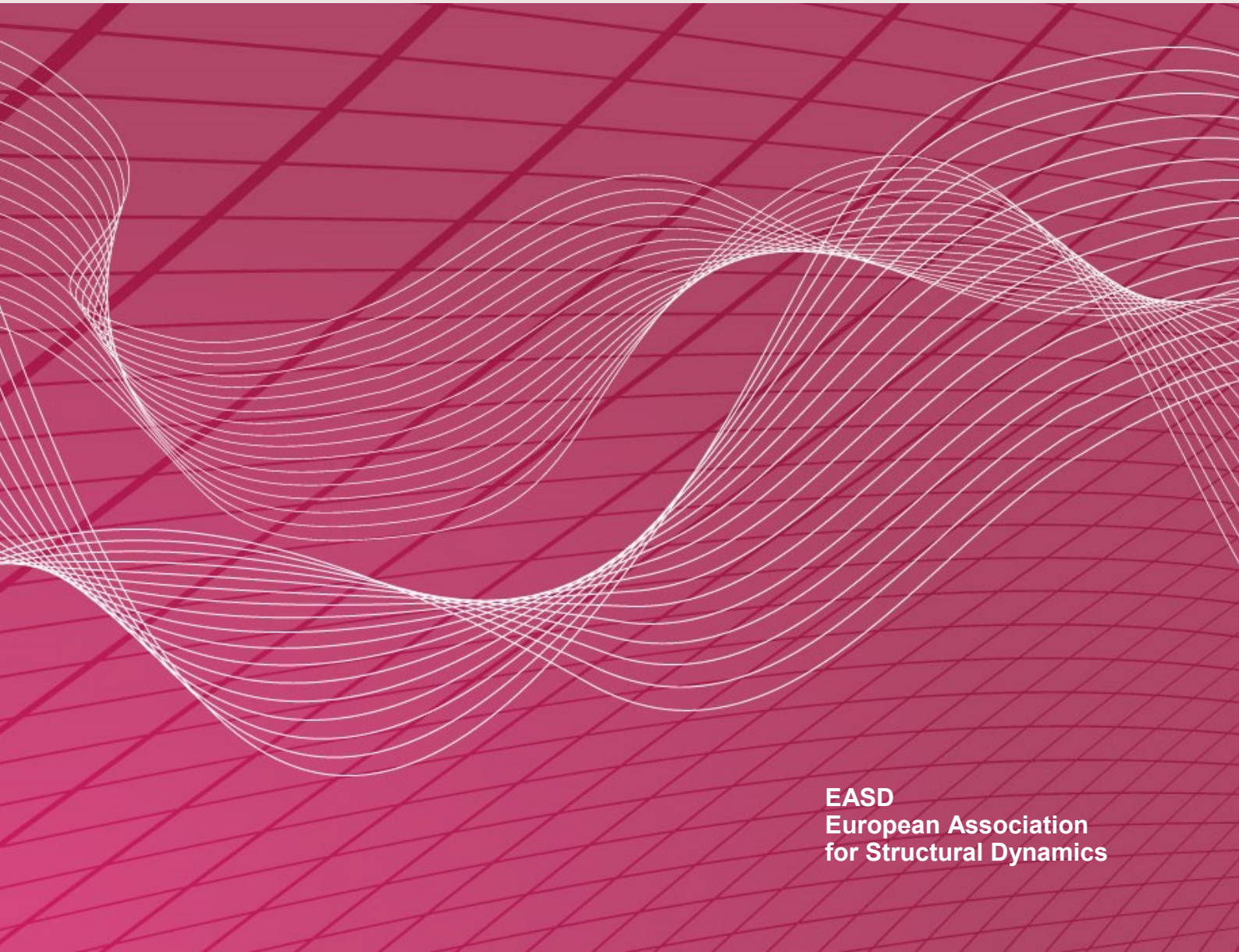

EASD
European Association
for Structural Dynamics

EURODYN 2020

Proceedings of the XI International Conference on Structural Dynamics

Streamed from Athens, Greece

23-26 November 2020

Edited by:

M. Papadrakakis

National Technical University of Athens, Greece

M. Fragiadakis

National Technical University of Athens, Greece

C. Papadimitriou

University of Thessaly, Greece

A publication of:

Institute of Structural Analysis and Antiseismic Research

School of Civil Engineering

National Technical University of Athens (NTUA)

Greece

EURODYN 2020

XI International Conference on Structural Dynamics

M. Papadrakakis, M. Fragiadakis, C. Papadimitriou (Eds.)

First Edition, September 2020

ISBN (set): **978-618-85072-2-7**

ISBN (vol II): **978-618-85072-1-0**

EURODYN 2020
XI International Conference on Structural Dynamics
M. Papadrakakis, M. Fragiadakis, C. Papadimitriou (eds.)
Athens, Greece, 23–26 November 2020

EFFECTS OF IMPULSIVE ACTIONS DUE TO SEISMIC JERK AND LOCAL FAILURES IN MASONRY STRUCTURES

Massimo Mariani[1] **and Francesco Pugi**[2]

[1] Studio Ricerche Applicate
06123 Perugia, Italy
ricercheapplicate@libero.it

[2] Aedes Software: Ricerca e Sviluppo
56028 San Miniato, Pisa, Italy
info@aedes.it

Keywords: masonry structures, seismic motion, jerk, impulsive forces

Abstract. *Recent studies [1-9] highlighted aspects of the seismic motion and the structural response which are usually ignored or not properly considered: the chaotic and spatial nature of the seismic motion, the importance of the vertical seismic component and its effect on the vulnerability of the structures. Considering seismic acceleration as a vector in space, the path outlined by the vector at each instant is the 3D representation of the accelerograms. The study of spatial accelerograms reveals interesting new aspects related to the variation of acceleration and the impulsive nature of the seismic motion. The seismic jerk (first derivative of acceleration and third derivative of displacement) is the fundamental component of the impulsive actions associated to high frequency content of the seismic motion. During the seismic event, the continuous variation of acceleration, in terms of modulus and direction, causes impulses (hammering, shaking, disconnection, etc.). In masonry structures they lead to local failures of the connections, disaggregation and damage accumulation with loss of ductility. Monitoring the seismic jerk in three directions may provide more significant information on the damage rather than monitoring the interstory drift. A design process is finally outlined: the study of the seismic motion impulsive content leads to solutions for structural retrofit aimed at strengthening masonry elements and improvement of connections.*

1 SEISMIC MOTION: ACCELERATION

The classic representation of a seismic event is a set of acceleration time series (also known as accelerograms) where ground acceleration is sampled in three mutually orthogonal directions.

By combining the three components of ground acceleration, one may plot a 3D path where each point is defined by the three components of the acceleration vector applied in the origin of the system. In this chart acceleration is not plotted against time but time is involved in indirect manner since each point corresponds to a different instant.

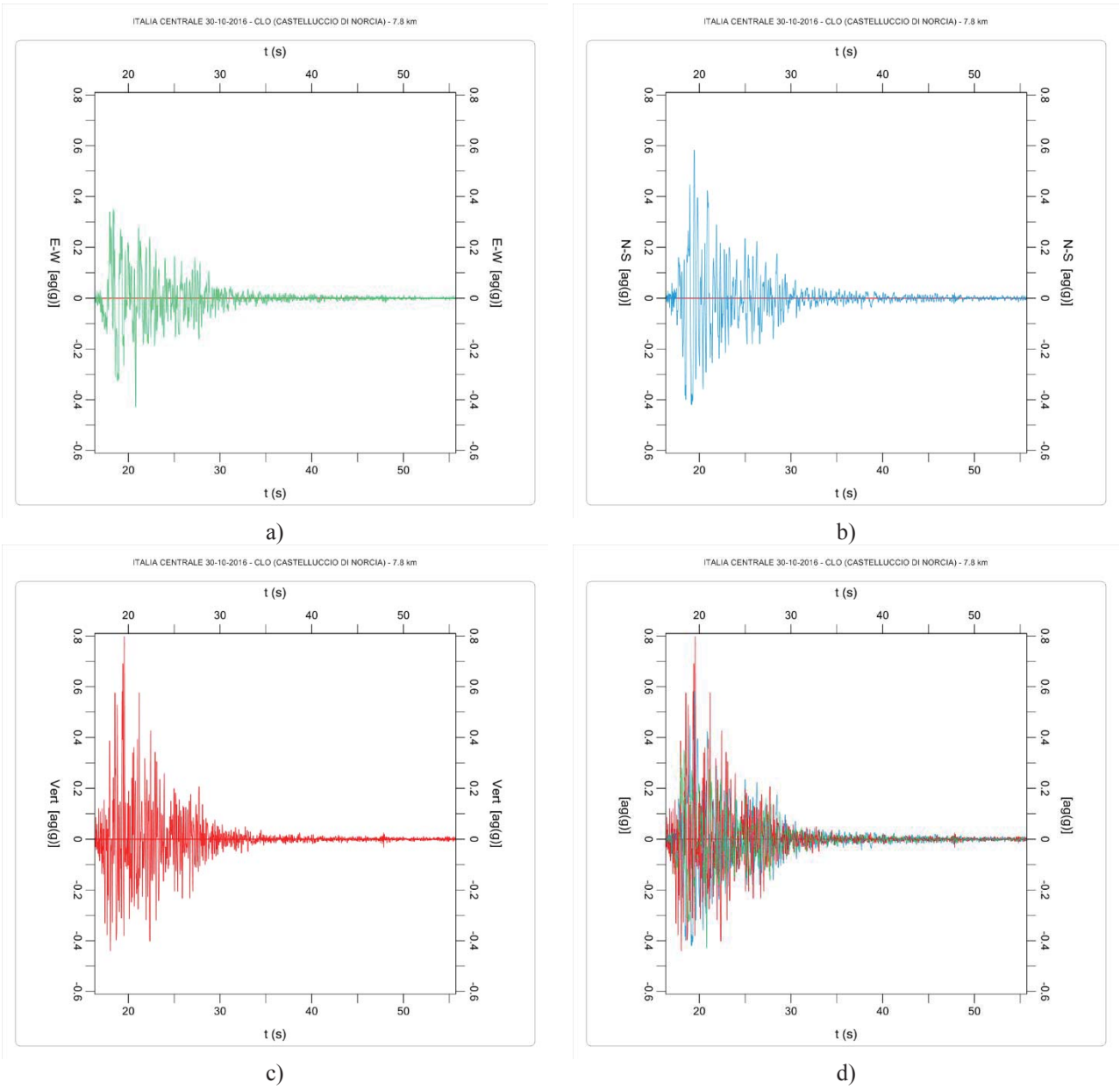

Figure 1. Traditional representation of accelerogram as time series: each component of ground acceleration is plotted against time. (a) EW component; (b) NS component; (c) Vertical component and (d) the three components overlaid in the same chart.

The 3D chart represents the seismic ground motion in a unified way: it highlights the simultaneity of the three components of ground acceleration and allows for direct comparison between them.

The graphic elaboration was carried out by means of the original software Seismic3D [10] specially developed for the purpose. Starting from the seismic event records, the software performs several elaborations aimed at studying the seismic ground motion.

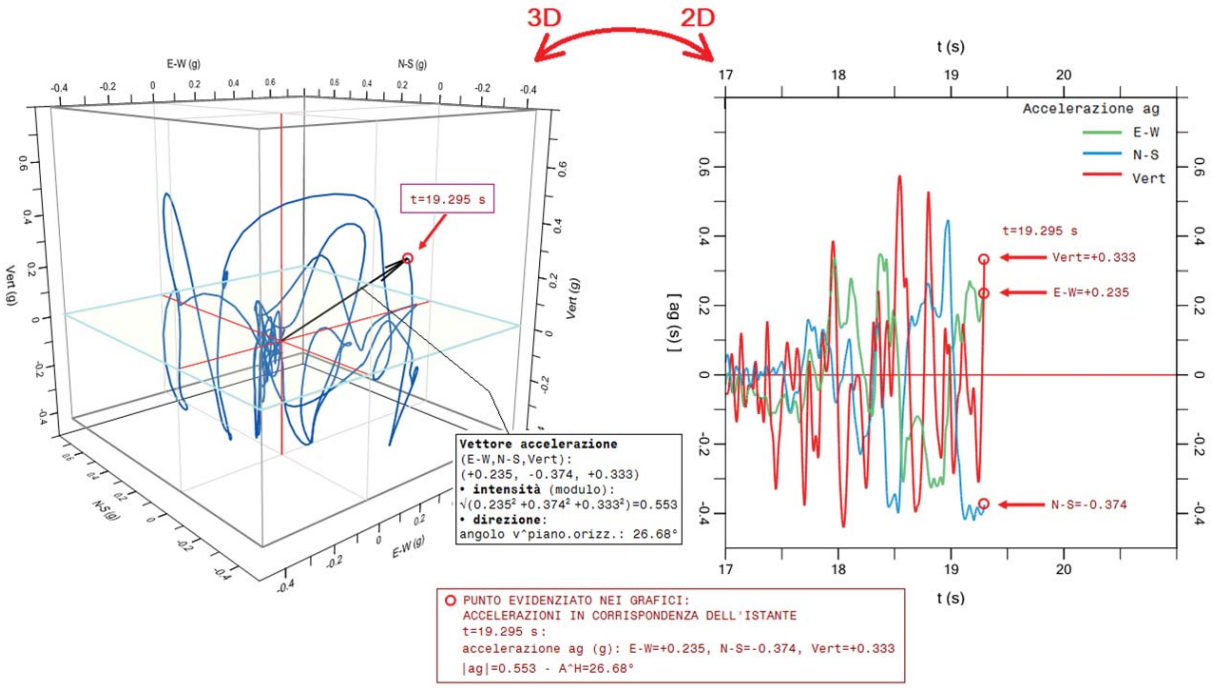

a)

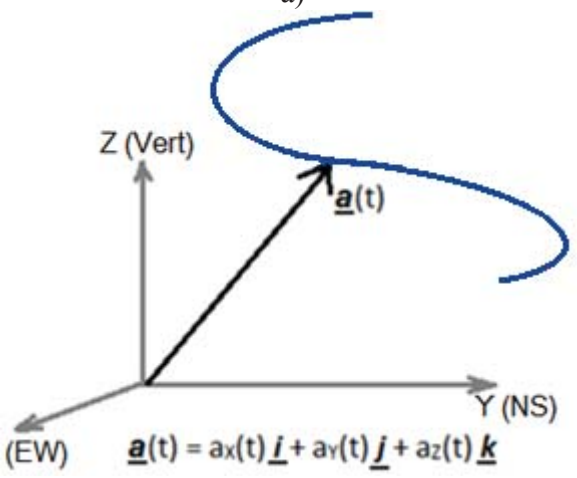

b)

Figure 2. (a) Evolution of the accelerogram from time series to 3D path (from plane to space) (b) Acceleration path outlined at any time by the acceleration vector

The 3D curve has the shape of a tangle: the more similar are the three components of acceleration the more compact and spherical is the tangle. In the following, the term “tangle” refers to the acceleration path when 2 or 3 components are considered.

Figures 1-2 show the evolution of the accelerogram from three separated time series in the plane (t, ag) to one 3D path in the space (a_gEW, a_gNS, a_gVert). The elaboration is based on

ground acceleration records at station CLO (Castelluccio di Norcia) from 30 October 2016 Norcia earthquake in Central Italy (mainshock).

The accelerograms in Figure 1 represent acceleration in a bracket duration: time span between the first and last peak exceeding 0.010 g.

At each instant, the acceleration vector is characterized by magnitude and direction. Magnitude (or modulus) is given by the square root of the sum of the squares of the three components. By ignoring one of the components, the 3D path is reduced to its projection on the plane of the other two components. For instance, by ignoring the vertical component we get a 2D path in the horizontal plane (a_gEW, a_gNS). Comparison between the 3D path and its projection on the horizontal plane highlights the contribution of the vertical component to total ground acceleration (Figure 3).

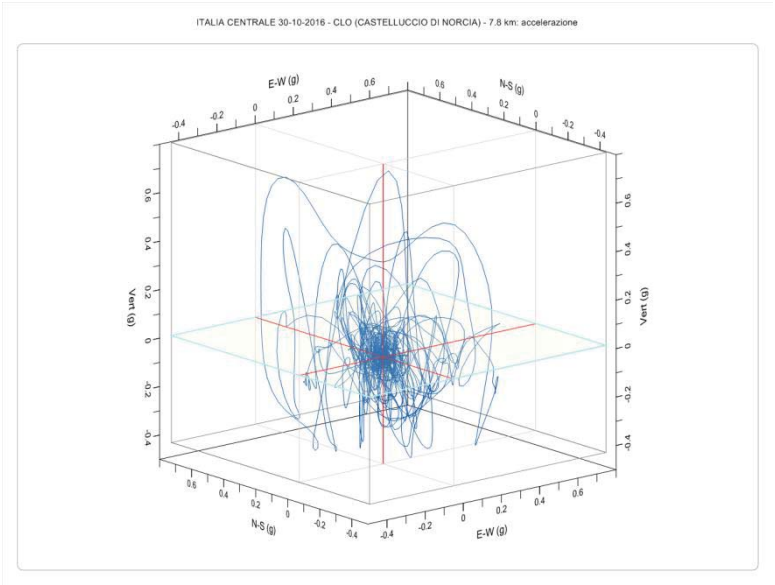

a)

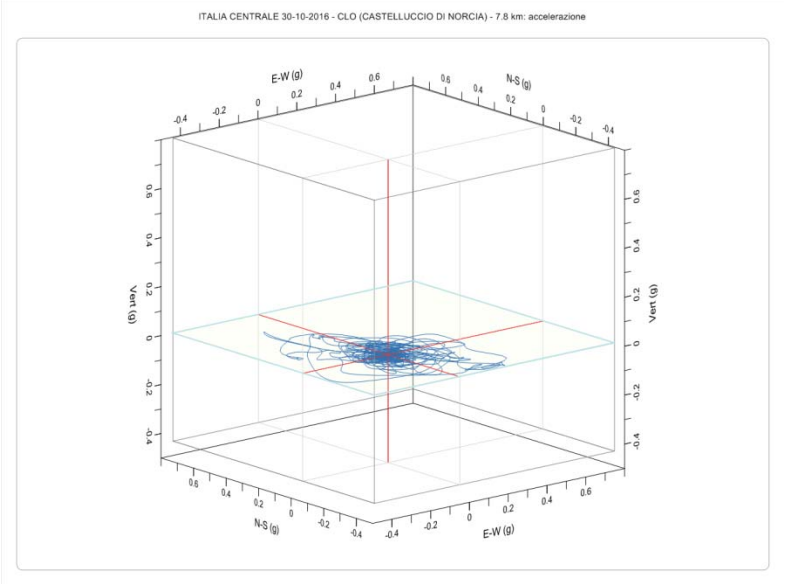

b)

Figure 3. Acceleration paths (or tangles).
(a) 3D path considering the three components; (b) 2D path ignoring vertical component

Figure 4 shows the projection of the 3D acceleration path (tangle) on the horizontal plane (a_gEW, a_gNS) and on the vertical planes (a_gEW, a_gVert) and (a_gNS, a_gVert). By comparing the 2D tangles one may observe that in this particular record the maximum values of the three acceleration components are very similar to each other.

The charts show the chaotic nature of the acceleration paths and the sharp variation in magnitude and direction of the acceleration vector. The plane accelerogram as time series shows the variation of one acceleration component at a time. Even when the time series of the three components are overlaid in the same chart, they cannot explicitly represent the real nature of the seismic motion. The ground acceleration records conceal a more complex reality which is finally revealed by their combination into the plot of the acceleration paths.

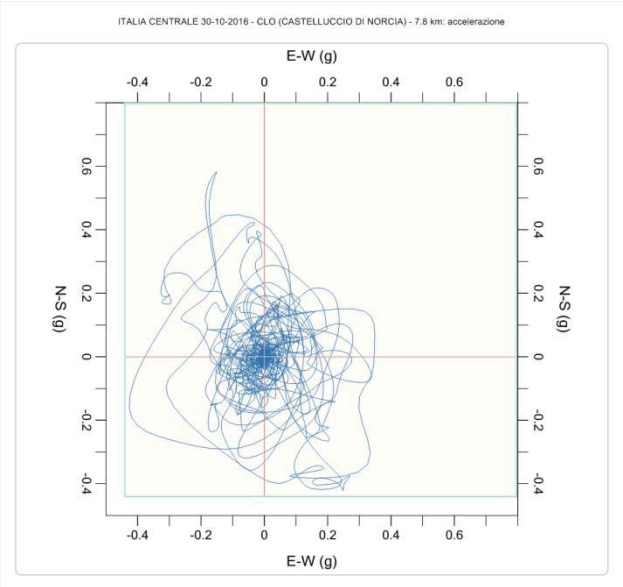

a)

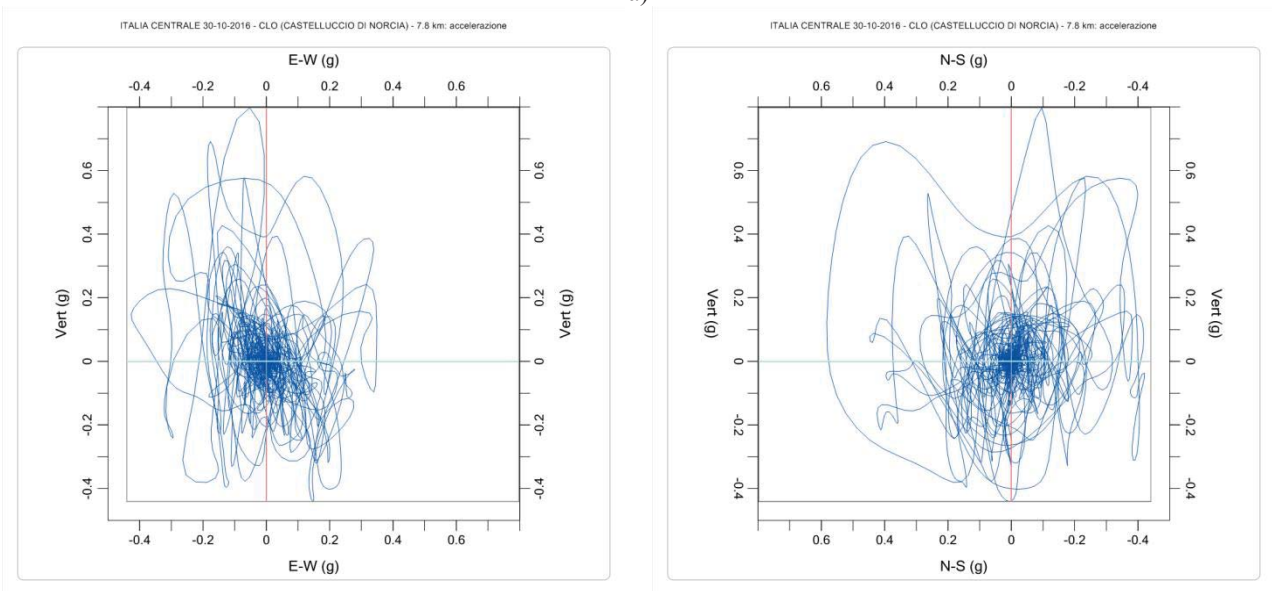

b) c)

Figure 4. Projections of the acceleration path on:
(a) horizontal plane (agEW,agNS); (b) vertical plane (agEW, agVert); (c) vertical plane (agNS, agVert)

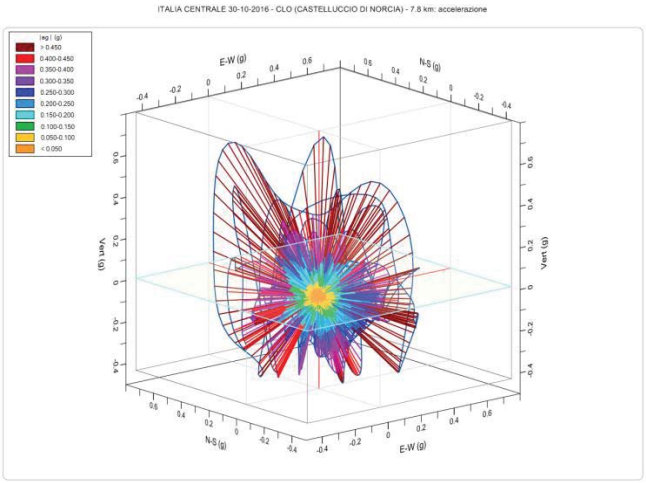

Figure 5. 3D Accelerogram: freezing motion of acceleration vector with color scale based on its magnitude

An interesting re-elaboration of the 3D chart can be obtained by "freezing" the motion of the acceleration vector at given time intervals, visualized with a color scale based on its magnitude (Figure 5).

As can be seen in Figure 5, the highest accelerations correspond to the "borders" of the path (characterized by dark red vectors) but the central core associated to lower accelerations (yellow or orange vectors) appears very dense showing countless variations in magnitude and directions which characterize a significant part of the seismic event.

To better understand the level of complexity one could zoom in the central core. Figure 6 shows the core in different levels of magnification. In order to reach this level of details, the acceleration record has been considered in a wide bracket duration, the time span between the first and last peak exceeding 0.005 g (15.385 s - 57.360 s, duration 41.985 s). In Figure 7 the same sequence is presented in the vertical plane (a_gNS, a_gVert).

These figures recall the fractals: whatever the scale, the curve always presents the same characteristics.

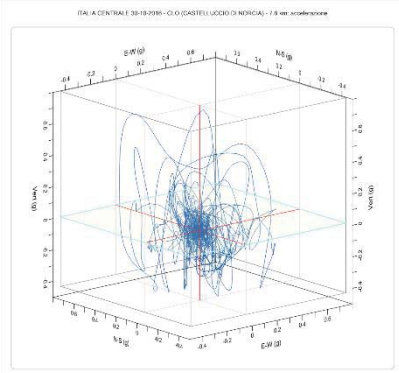

a) full box

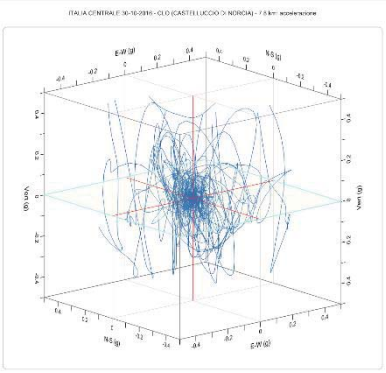

b) limit box: 0.500 g

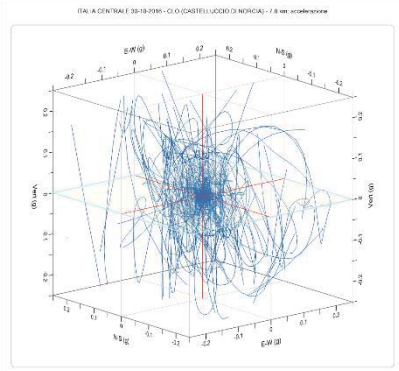

c) limit box: 0.250 g

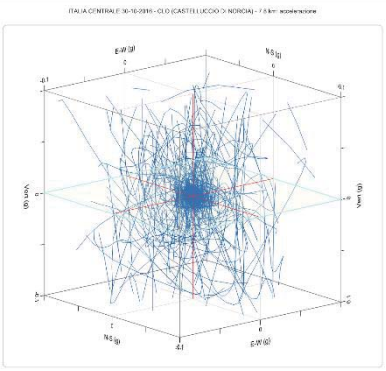

d) limit box: 0.100 g

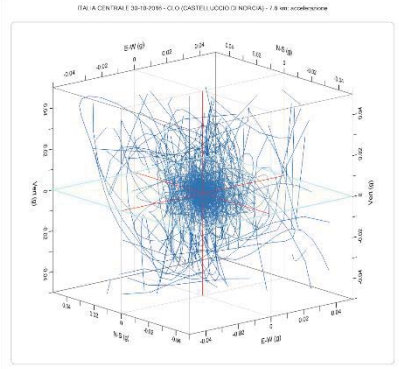

e) limit box: 0.050 g

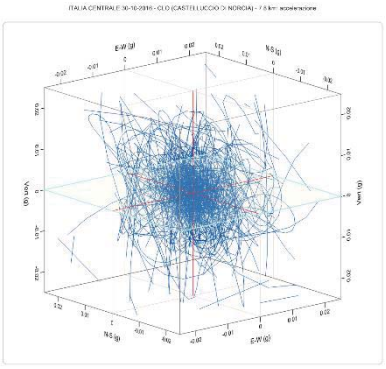

f) limit box: 0.025 g

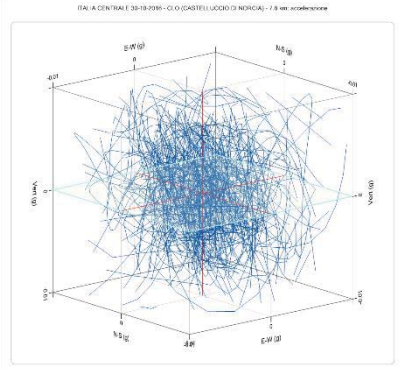

g) limit box: 0.010 g

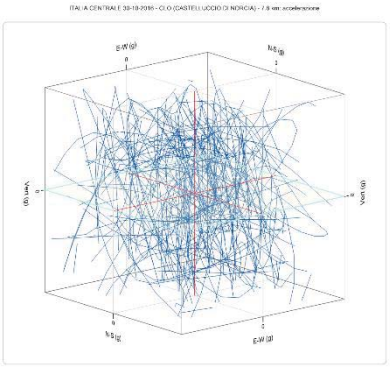

h) limit box: 0.005 g

Figure 6. Different levels of magnification of the acceleration path: 3D view

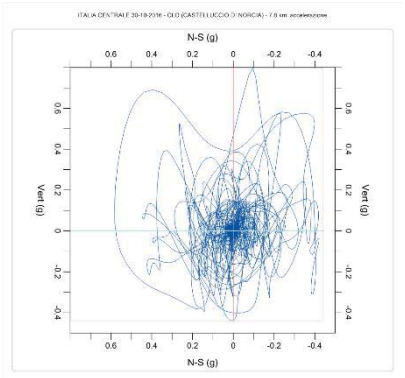

a) full box

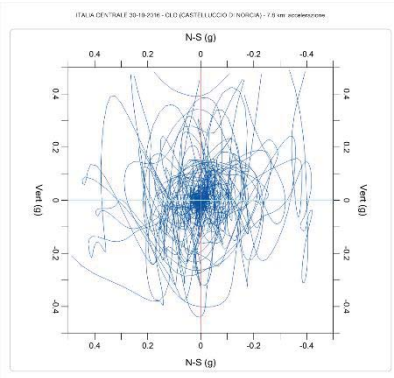

b) limit box: 0.500 g

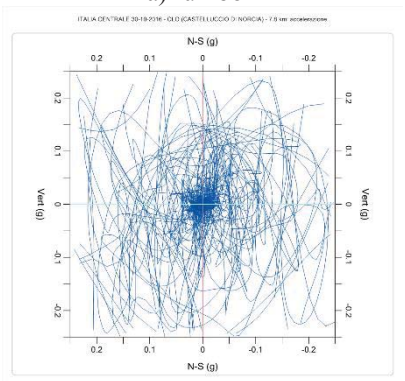

c) limit box: 0.250 g

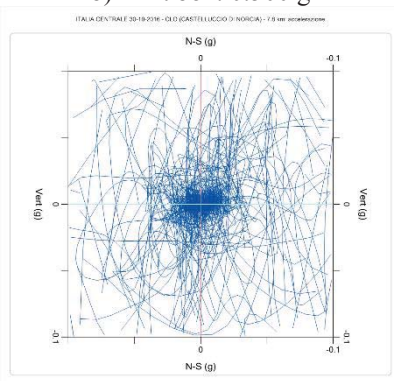

d) limit box: 0.100 g

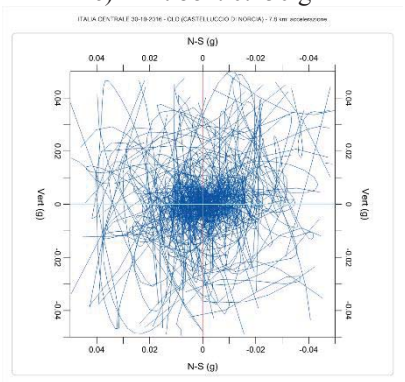

e) limit box: 0.050 g

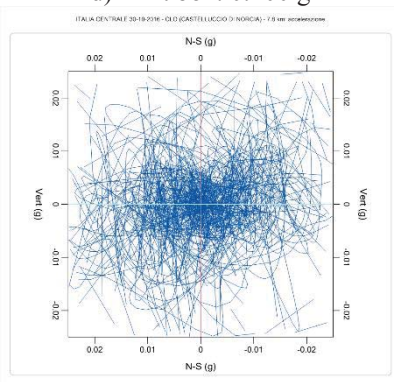

f) limit box: 0.025 g

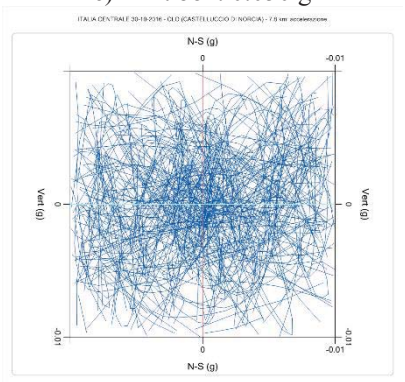

g) limit box: 0.010 g

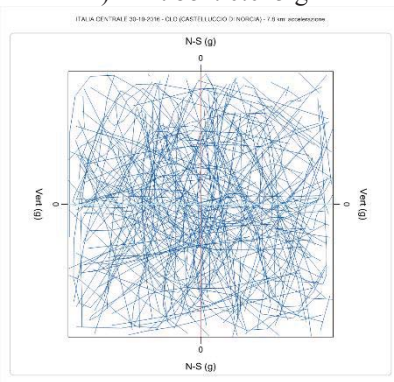

h) limit box: 0.005 g

Figure 7. Different levels of magnification of the acceleration path: projection on vertical plane NS-Vert

The charts show what happened in Castelluccio di Norcia on 30 October 2016 in about 40 seconds. Considering the bracket time span between the first and last acceleration peak exceeding 0.250 g, we obtain the chart shown in Figure 8 for a time span of 6.48 s (17.435 s to 23.915 s). The red labels in the chart point out the acceleration reached at each second. In this way "time" re-appears in the chart highlighting the progression of the path.

In 6 seconds, the ground motion was characterized by violent accelerations especially in the vertical direction. The ground accelerations generated inertial and impulsive forces which caused collapses and severe damages to the buildings. A destruction happened in a very short time interval caused by a chaotic event, extremely different in its nature from the static actions that stress the buildings under operating conditions.

The 3D accelerograms, that are the paths outlined by the acceleration vector, indicate a new perspective: studying the shape of the curves and their evolution throughout the duration of the seismic event. The continuous changes of the acceleration vector in terms of magnitude and direction suggest to further investigate on the variation of acceleration. In fact, the safety verification applied in terms of resistance and deformation under inertial forces, may not be enough to fully describe the structural response. Assessment of the structural capacity cannot ignore verifications on the impulsive effects, that are the forces related to the short time intervals in which accelerations change, increase, decrease or change sign.

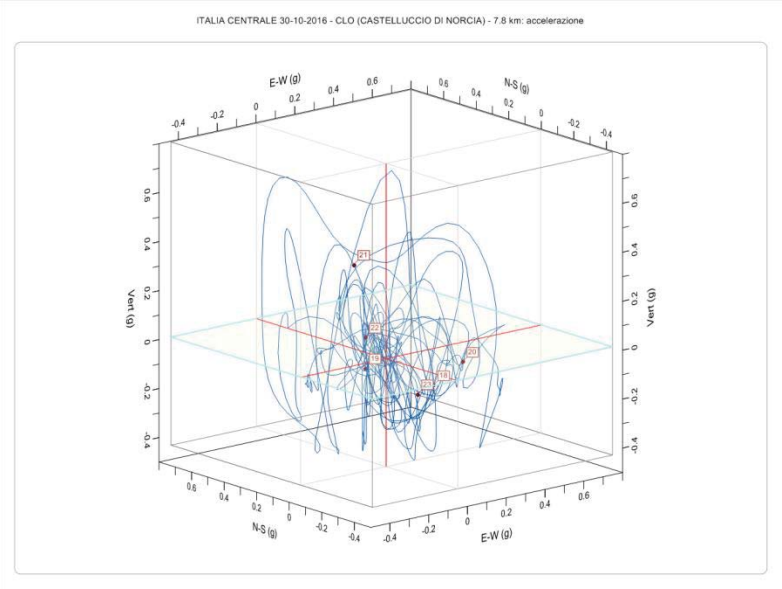

Figure 8. 3D Accelerogram at station CLO during 2016 Norcia mainshock: about 6 seconds while acceleration is above 0.25 g

2 JERK: FIRST DERIVATIVE OF ACCELERATION

The time derivative of acceleration (TDoA), that is the velocity of acceleration or the third derivative of displacement, is referred to as jerk and associated to the symbol j:

$$\boldsymbol{j} = \frac{d\boldsymbol{a}}{dt} \tag{1}$$

Since force acting on a body is equal to mass times acceleration, the jerk is related to the variation of the force acting on the body:

$$\boldsymbol{F} = m\boldsymbol{a} \Rightarrow \boldsymbol{j} = \frac{\left(\frac{d\boldsymbol{F}}{dt}\right)}{m} \tag{2}$$

In absence of jerk, a mass in constant acceleration is subject to static loading (constant force) and in this condition vibrations cannot occur. Therefore, when a body in motion undergoes vibration, jerk is always there.

Tong et al. (2005) [11] investigated on seismic jerk stating from the need of obtaining quantitative understanding about its amplitude, duration and frequency content. The study is based on records from the 1999 Chi-Chi Earthquake in Taiwan (M_W 7.6, 17:47, 20 September 1999) and one of its aftershocks (M_W 6.2, 00:14, 22 September 1999). At that time, jerk sensors were not widely available; therefore, jerk time series were obtained from ground acceleration records via numerical methods. This methodology, which can be applied to other seismic events where jerk records are not available, was implemented in the software Seismic 3D [10]

Seismic acceleration is a discrete signal, therefore seismic jerk can be calculated by the following mi-point differentiation formula:

$$j(t_i) = \frac{a(t_{i+1}) - a(t_{i-1})}{2\Delta t} \quad (i = 2, \dots, N-1) \tag{3}$$

where: $a(t_i)$ is the acceleration at instant t_i, N is the number of samples, Δt is the sampling period.

The formula is applied separately for each of the three components of the jerk vector **j.**

The accuracy of the jerk elaboration relies on the accuracy of the acceleration records and the sampling rate. Ground acceleration records of the main seismic events on the Italian territory are provided by ITACA [12] with a sampling period of 5 ms (200 Hz). The records are also corrected to reduce errors in high and low frequency; therefore, quality of the records is excellent for the purposes of this work.

At this point it comes naturally to represent the variation of jerk both as time series of its three components and as 3D path outlined by the jerk vector in space. In this way one can get graphs like the ones seen for acceleration.

In the 3D graph of the acceleration path it is worth noticing that the **j** vector is tangent to the path at each point.

Figure 9 shows the time series of the three jerk components at station CLO (Castelluccio di Norcia) from the 30 October 2016 Norcia earthquake. Table 1 summarize the maximum amplitude of acceleration (PGA) and jerk (PGJ) for each of the three components, and the instant in the record when they occur.

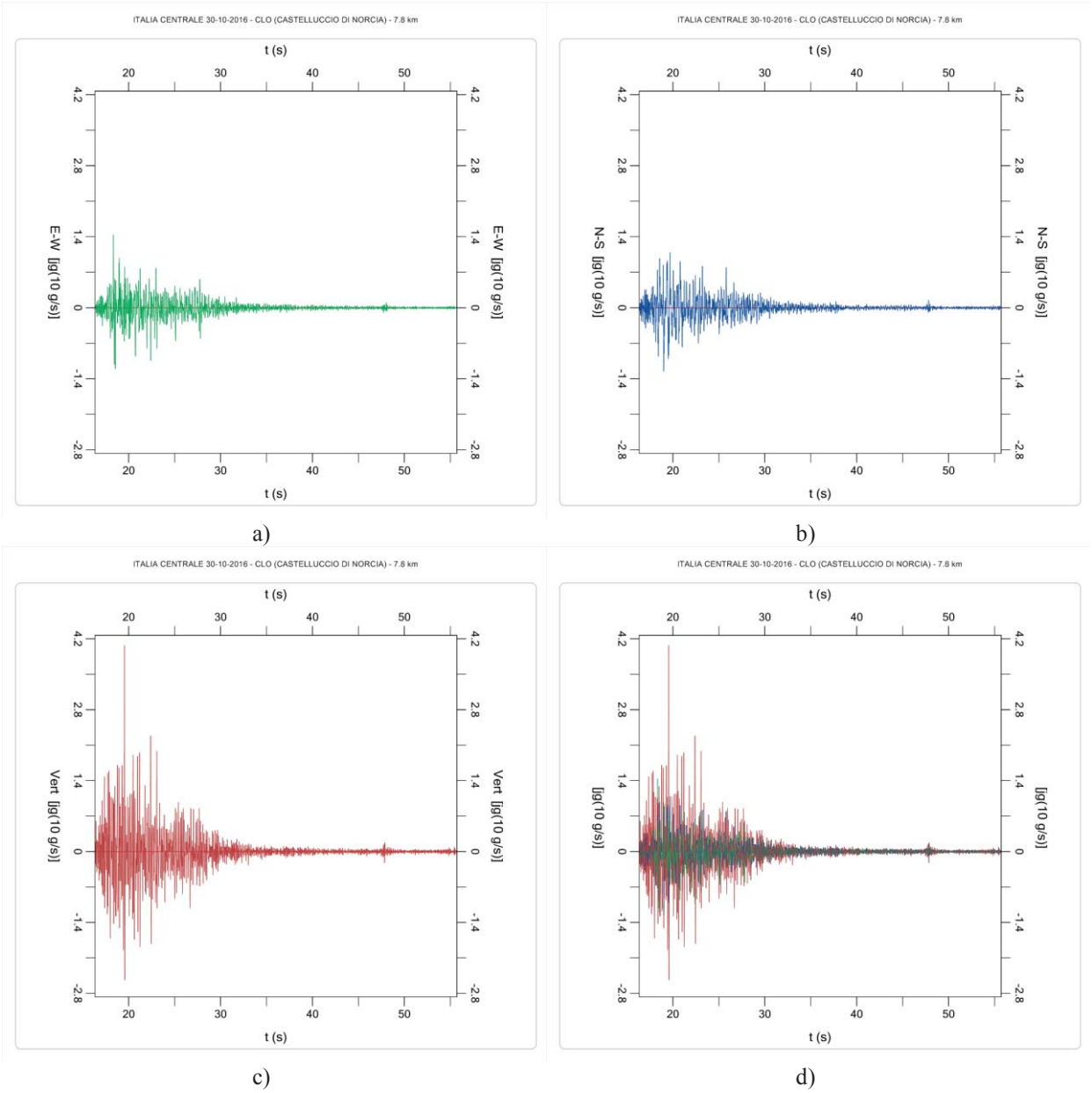

Figure 9. Jerk time series: each component of ground jerk plotted against time. (a) EW component; (b) NS component; (c) Vertical component and (d) the three components overlaid in the same chart.

	EW	t (s)	NS	t (s)	Vert.	t (s)
PGA (g)	0.427	20.775	0.583	19.445	0.797	19.560
PGJ (g/s)	14.36	18.335	12.50	18.995	40.70	19.540

Table 1. Station CLO (Castelluccio di Norcia), 30 October 2016 Norcia earthquake. Maximum acceleration (PGA) and maximum jerk (PGJ) for each of the three components and corresponding time instant

The maximum values of jerk (PGJ) occur at different instants of time than the ones of acceleration (PGA). They occur in a time interval between 18 s and 21 s and there is not a clear relationship with the occurrence of PGA values in the three directions.

In this event both vertical acceleration and jerk are rather strong with respect to the horizontal component. Vertical acceleration almost reached 0.8 g (Figure 1) and the vertical PGJ of about 40 g/s (Figure 9) is almost double than the horizontal ones.

In order to understand the relationship between acceleration and jerk, let us consider the time series of their vertical component focusing on a small time interval between 19.3 s and 19.8 s (0.5 s) in which both PGA and PGJ occur.

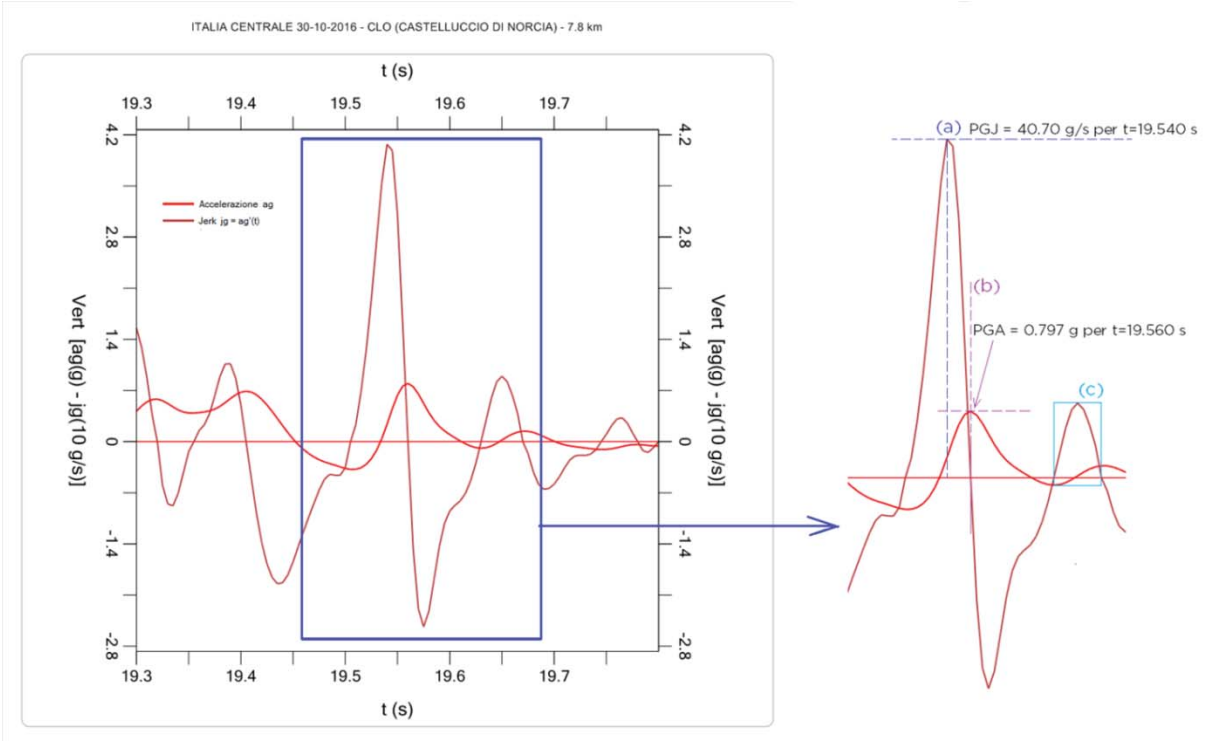

Figure 10. Comparison between acceleration and jerk time series. The detail on the right shows how the points where jerk is zero correspond to local maximum or minimum of acceleration.

Since jerk is the first derivative of acceleration it is equal to zero when acceleration shows a local maximum or minimum.

The detail in Figure 10 highlights (a) the absolute maximum of jerk (PGJ); (b) the absolute maximum of acceleration correspondent (like other local maximum) to zero in jerk; (c) the sector between two consecutive zeros of jerk correspondent to local minimum and maximum of acceleration.

Figure 11 shows the time series of acceleration and jerk for the three components in the time span between 18.0 s and 21.0 s. Jerk time series feature a higher number of fluctuations between positive and negative values: this is even more evident from the detail in Figure 12. Throughout the seismic event, the secondary fluctuation of acceleration corresponds to significant jerk peaks of alternate sign. The operation of derivation generates a “jerky” function characterized by denser peaks, that is in strict terms, by higher frequencies.

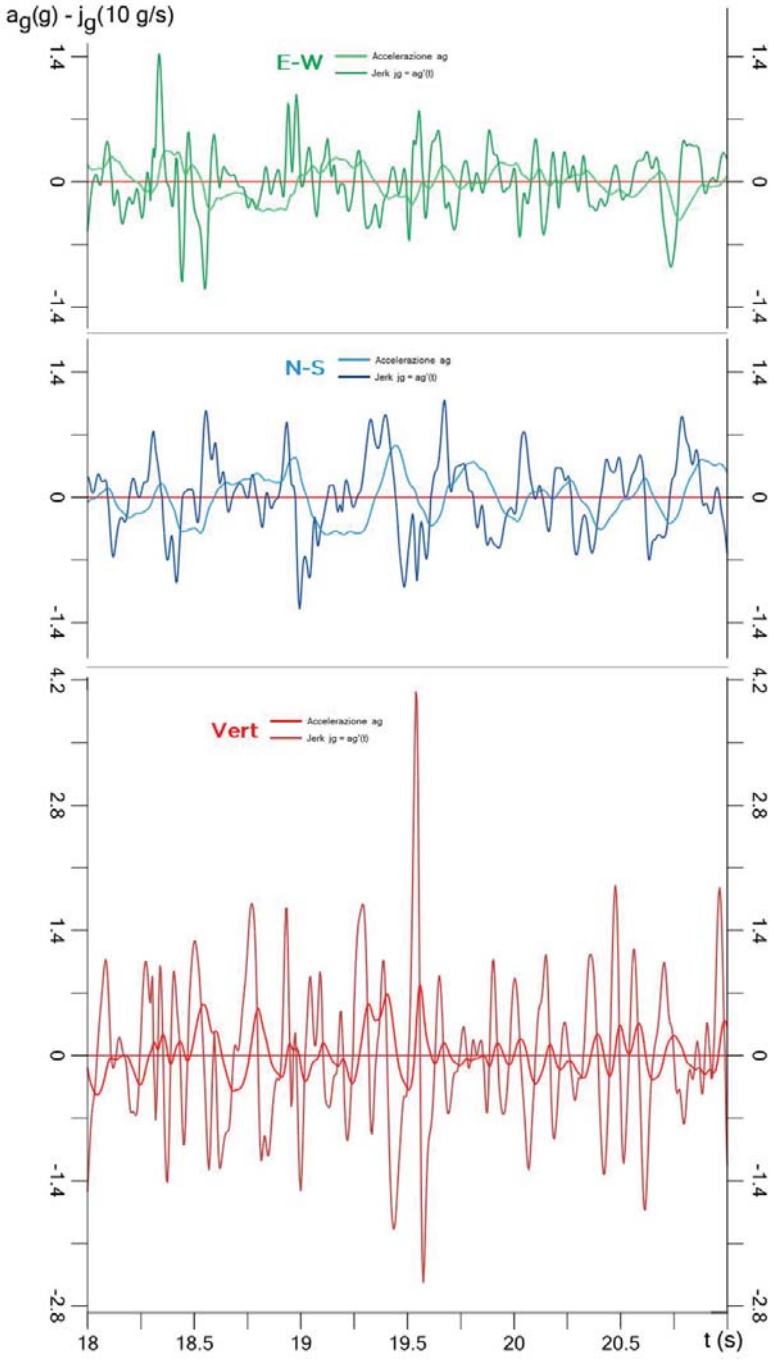

Figure 11. Acceleration and jerk time series for the three components (EW, NS, Vert)

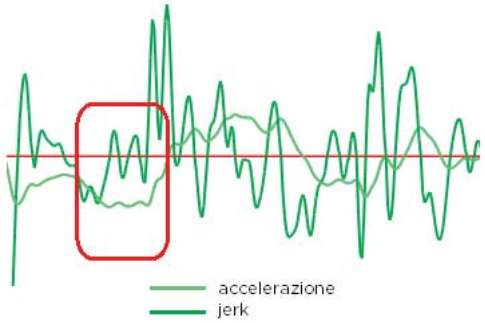

Figure 12. Secondary fluctuation of acceleration correspondent to jerk peaks

The graphs of jerk variation in space as the 3D path outlined by the **j** vector are similar to the ones already seen for acceleration. Comparison between acceleration and jerk paths is given in Figure 13 (3D view), Figure 14 (EW-NS plane), Figure 15 (EW-Vert plane) and Figure 16 (NS-Vert plane).

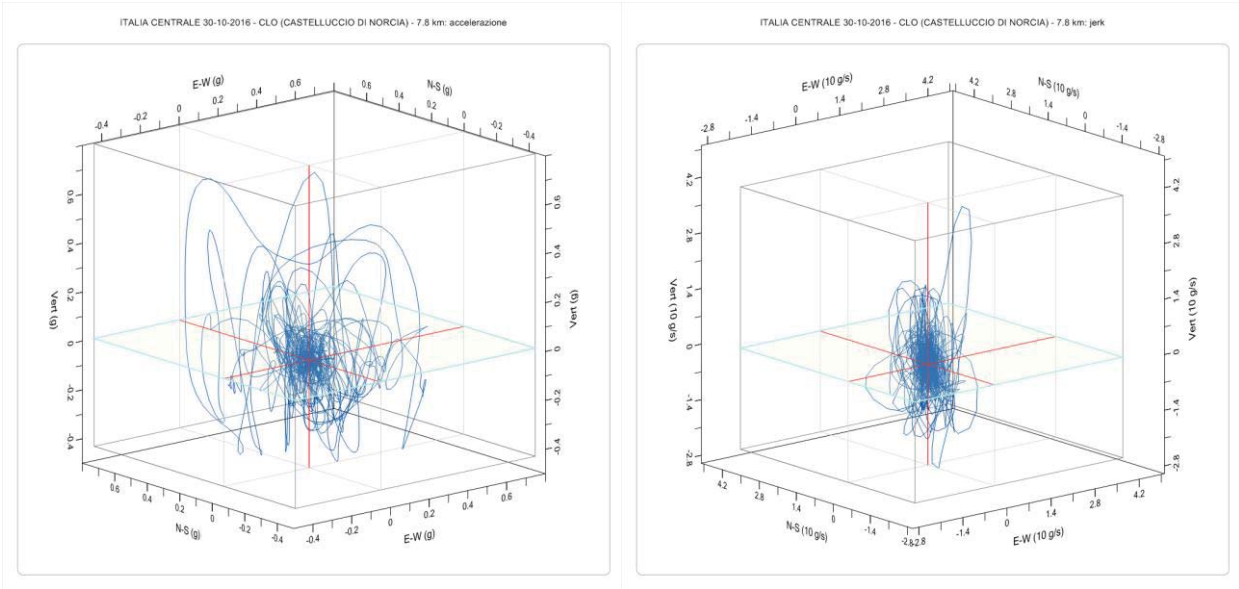

a) b)

Figure 13. Comparison between (a) acceleration and (b) jerk paths: 3D view

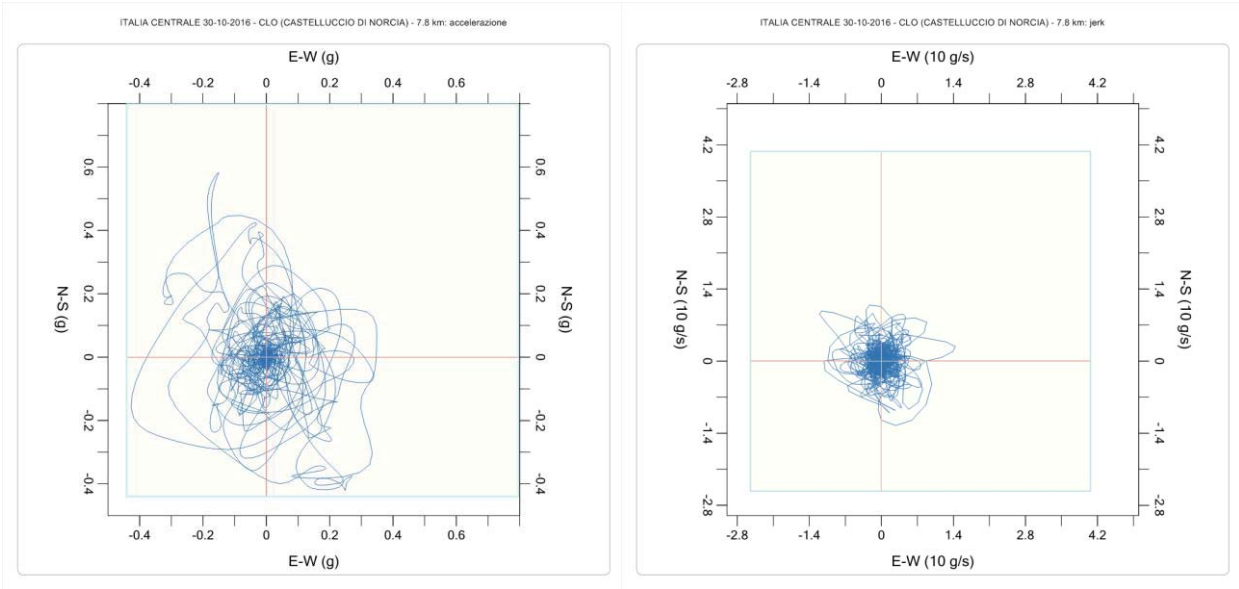

a) b)

Figure 14. Comparison between (a) acceleration and (b) jerk paths: projection on horizontal plane EW-NS

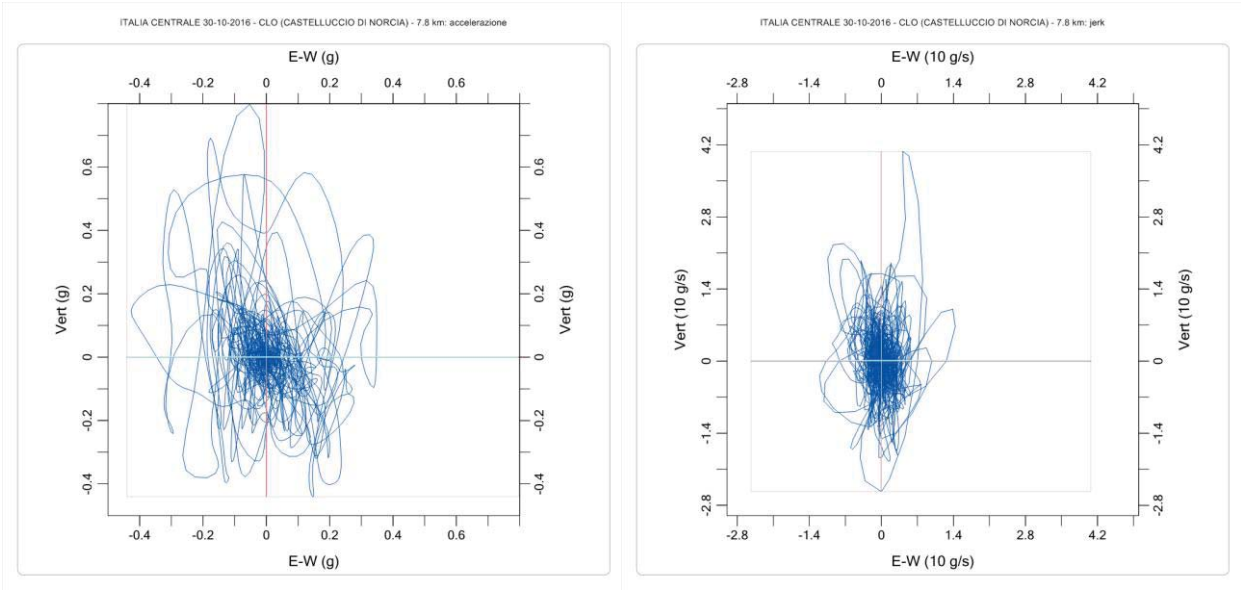

a) b)

Figure 15. Comparison between (a) acceleration and (b) jerk paths: projection on vertical plane EW-Vert

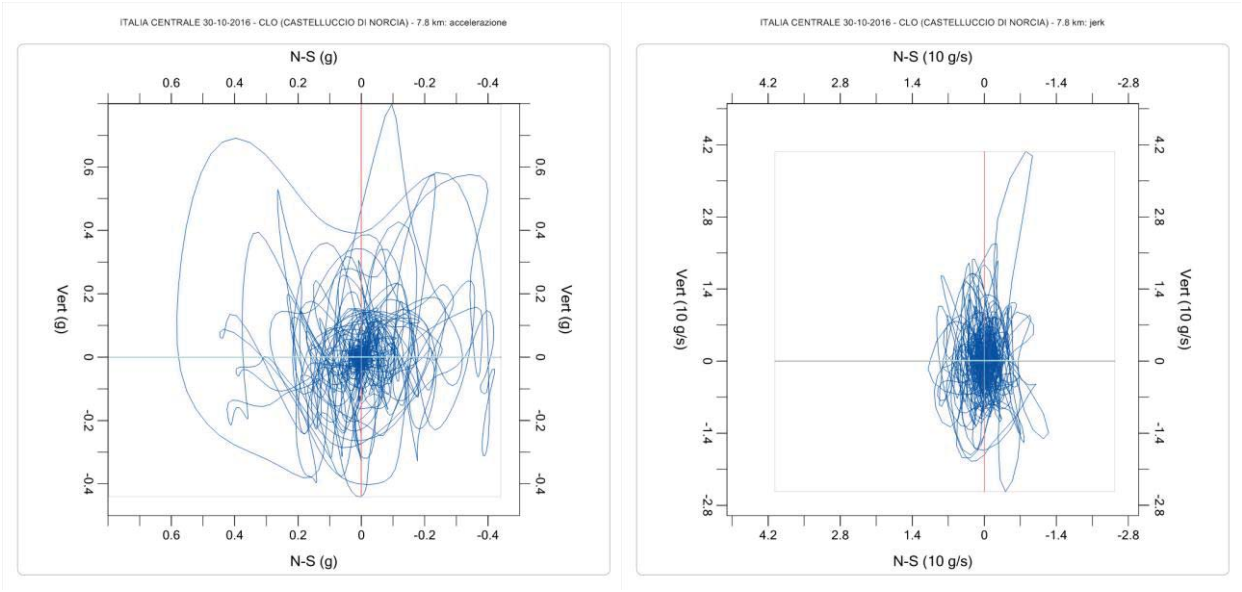

a) b)

Figure 16. Comparison between (a) acceleration and (b) jerk paths: projection on vertical plane NS-Vert

All the views highlight that the jerk tangle is denser than the acceleration one: this is in agreement with what previously noted in the comparison between acceleration and jerk time series. The projection of the jerk tangle on the vertical planes appears stretched in the vertical direction and this points out the importance of the vertical seismic component.

It is worth noticing that even the jerk paths feature a fractal type shape. Figure 17 shows different levels of magnification of the jerk path, from the box which envelopes the curve to the 0.5 g/s box.

This proves the chaotic nature of the represented phenomenon: the zoom in the core of the paths clearly highlights that, although the amplitude is lower, the number of fluctuations is

very high: this leads to the hypothesis that the phenomenon may disrupt the intimate constitutive bonds of the materials.

Since jerk is the first derivative of acceleration, a good way to understand its evolution is to represent the $\boldsymbol{j}$ vector on the acceleration path. Applying differential geometry of curves in $\mathbb{R}^3$, it can be proved that at the i-th instant t_i the vector $\boldsymbol{j}(t_i)$ is tangent to the curve in the point $\boldsymbol{a}(t_i)$. The modulus of vector $\boldsymbol{j}$ is given by the square root of the sum of the squares of its three components, each one being the time derivative of the correspondent acceleration component evaluated at instant t_i:

$$|\boldsymbol{j}(t_i)| = j_{3D}(t_i) = \sqrt{j_{EW}^2(t_i) + j_{NS}^2(t_i) + j_{Vert}^2(t_i)} \quad (i = 2, \dots, N-1)$$
$$where: \qquad (4)$$
$$j_{EW}(t_i) = \left.\frac{da_{EW}(t)}{dt}\right|_{t=t_i}, \quad j_{NS}(t_i) = \left.\frac{da_{NS}(t)}{dt}\right|_{t=t_i}, \quad j_{Vert}(t_i) = \left.\frac{da_{Vert}(t)}{dt}\right|_{t=t_i}$$

Jerk $\boldsymbol{j}$ is the rate of change of acceleration, that is, velocity of acceleration: there is complete analogy with velocity $\boldsymbol{v}$ as rate of change of displacement. Figure 18 shows the jerk vector on the 3D accelerogram (acceleration path). The bracket duration is defined as the time span between the first and last acceleration peak exceeding 0.250 g (17.435 – 23.915 s). The j vector is represented at instant t = 19.375 s by a red arrow, which of course is tangent to the curve from any point of view.

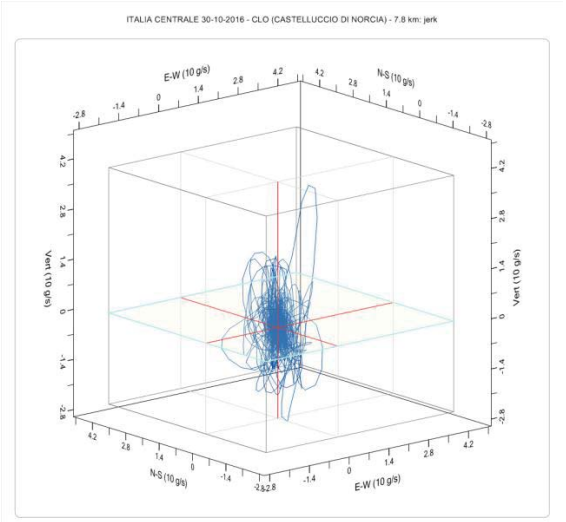

a) full box

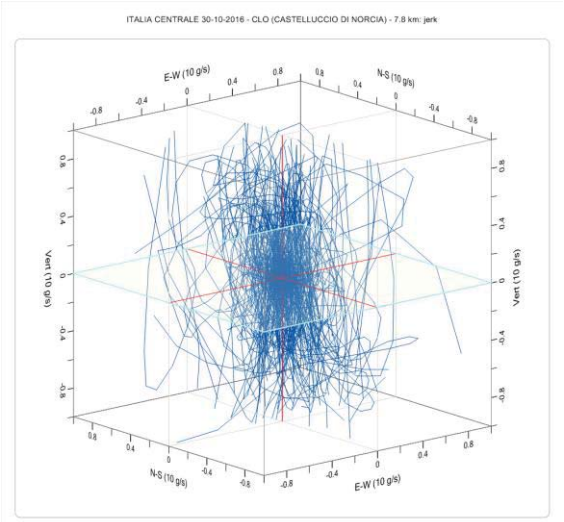

b) limit box: 10 g/s

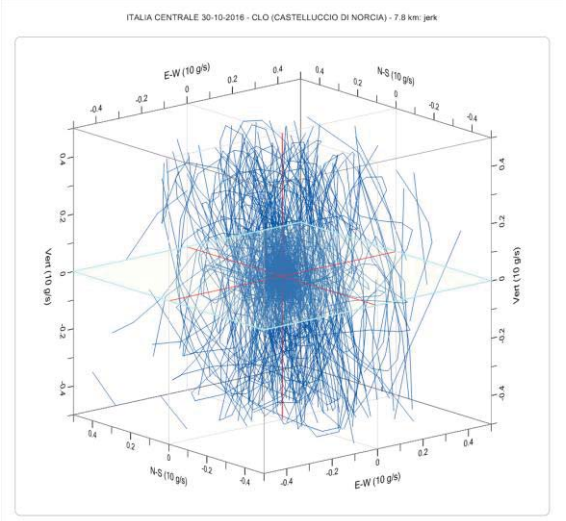

c) limit box: 5 g/s

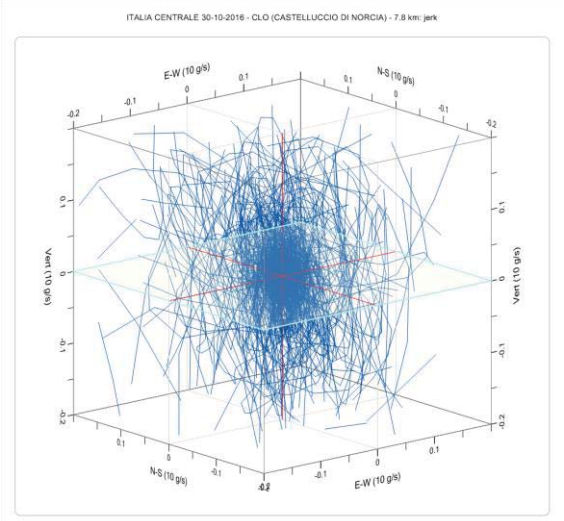

d) limit box: 2.5 g/s

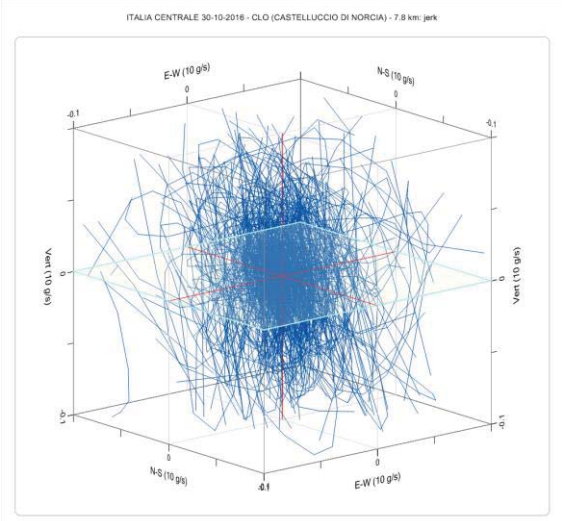

e) limit box: 1 g/s

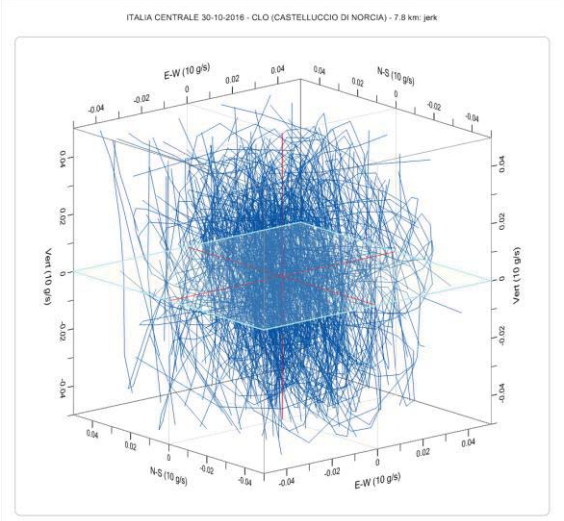

f) limit box: 0.5 g/s

Figure 17. Different levels of magnification of the 3D jerk path

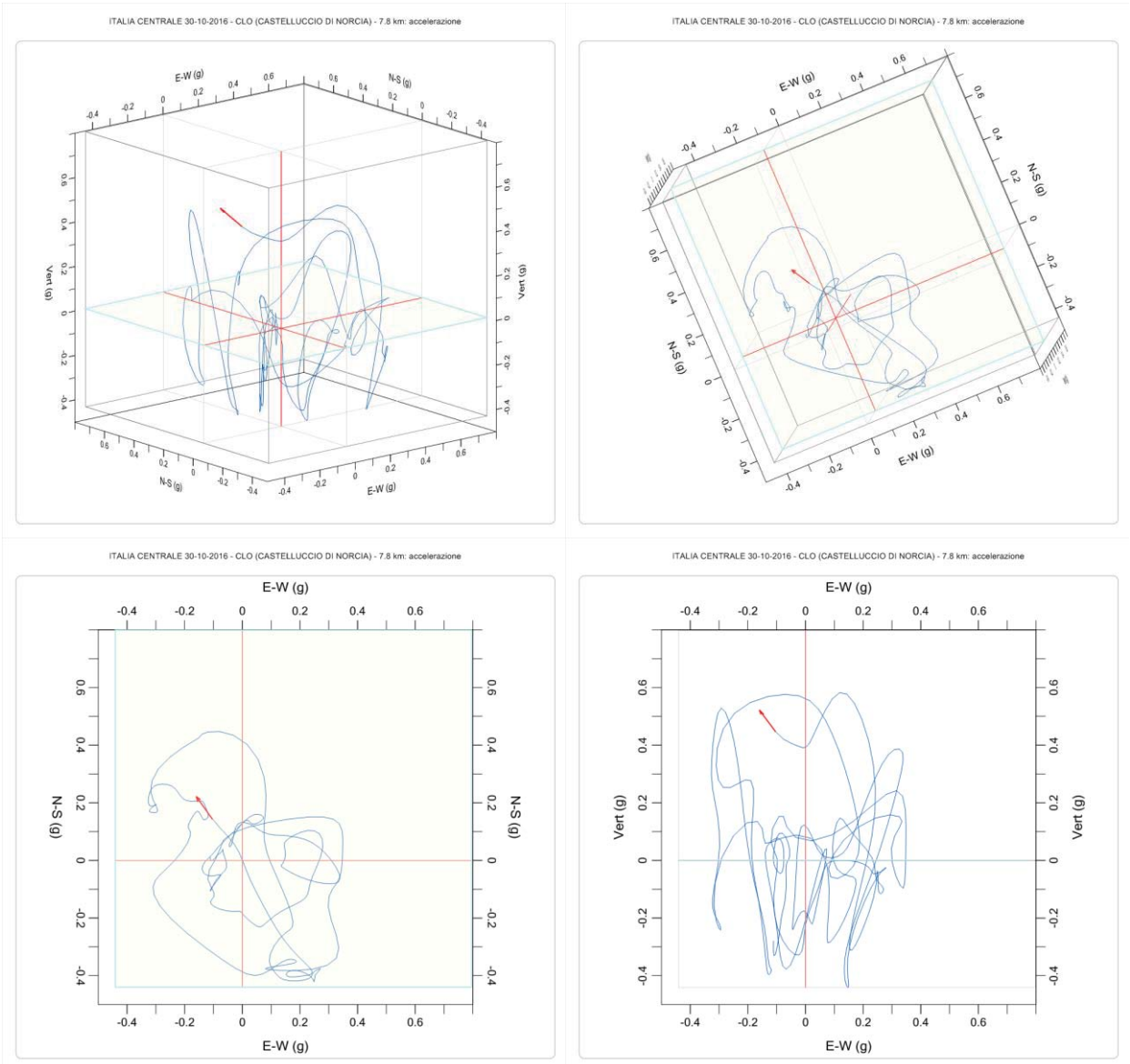

Figure 18. The jerk vector on the 3D accelerogram (acceleration path) from different points of view

Considering acceleration and jerk as vectors in space, PGA and PGJ may not only be expressed for the three separated components but also with respect to the magnitude (modulus) of the vectors. Therefore, Table 2 updates Table 1 with the inclusion of global PGA and PGJ and the instant when they occurred.

	EW	t (s)	NS	t (s)	Vert.	t (s)	3D	t (s)
PGA (g)	0.427	20.775	0.583	19.445	0.797	19.560	0.829	19.410
PGJ (g/s)	14.36	18.335	12.50	18.995	40.70	19.540	41.69	19.540

Table 2. Station CLO, 30 October 2016 Norcia mainshock. Peak ground acceleration (PGA) and peak ground jerk (PGJ). Three separated components and magnitude of the 3D vectors

Peaks of vectors magnitude are of course higher than the peaks of the singular components and they generally occur at different time instants. The maximum effects of seismic ground motion, both in terms of acceleration and jerk, did not occur along one of the three axes of the reference system (X,Y, Z) but along a random direction in space.

Figure 19 shows the time series of acceleration and jerk magnitude (3D) for two different bracket duration. The maximum values of these time series are given in Table 2 as 3D values.

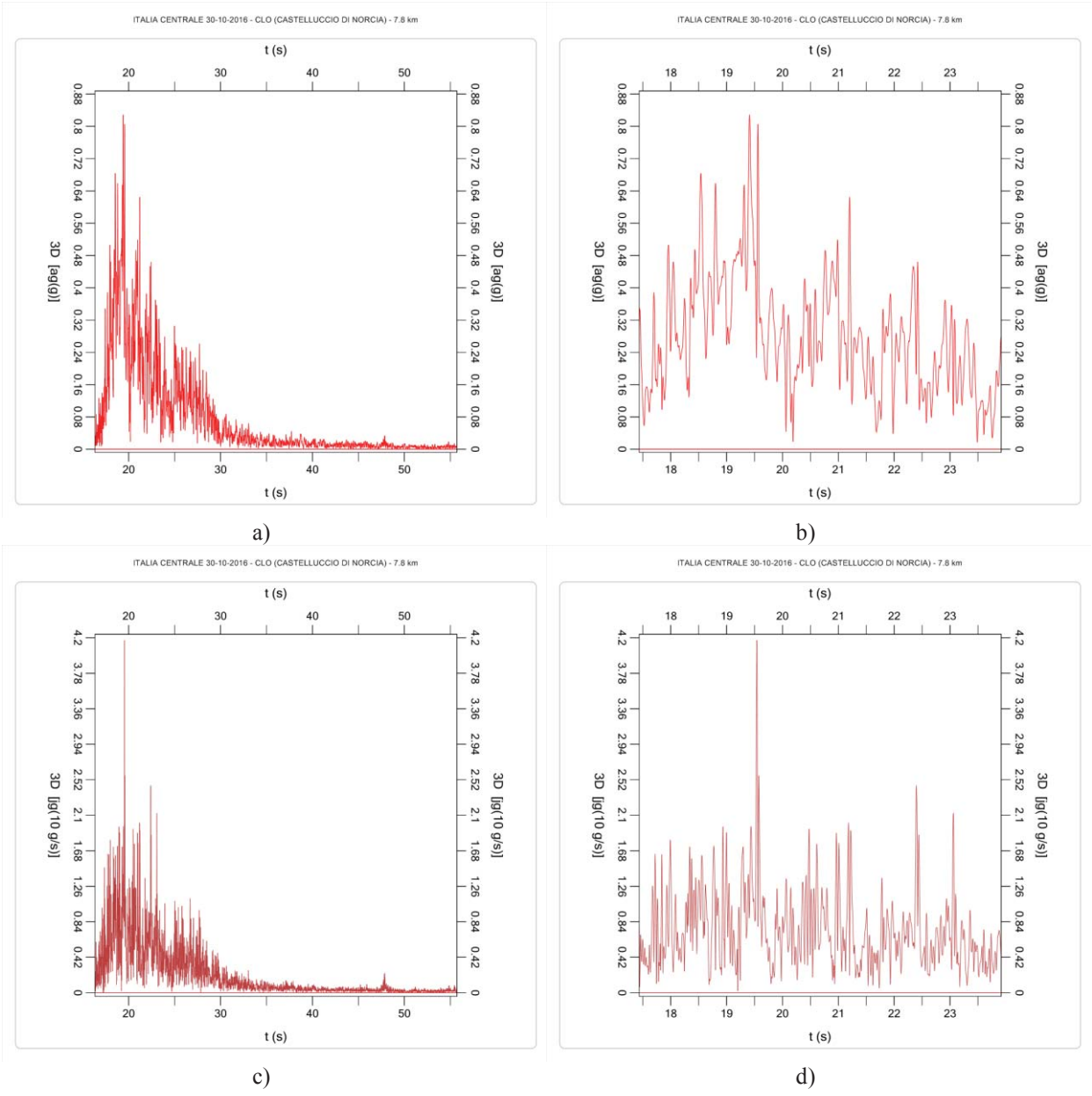

Figure 19. Station CLO, 2016 Norcia mainshock: acceleration and jerk 3D magnitude time series.
(a, b) acceleration time series; (c, d) jerk time series;
(a, c) time series cut-of at the acceleration threshold of 0.010 g (16.330 - 55.715 s);
(b, d) time series cut-of at the acceleration threshold of 0.025 g (17.435 - 23.915 s).

3 IMPULSIVE FORCES DUE TO JERK

During a seismic event, ground acceleration varies quickly, and the correspondent inertial forces also fluctuate in short time intervals of the order of few milliseconds. This sharp variation causes "jolts", that is, impulsive forces that act very briefly. Therefore, jerk could become a useful parameter for structural analysis and design if it is considered with the corresponding impulsive forces. A new approach is introduced below.

The study is based on ground acceleration records at station CLO (Castelluccio di Norcia) from 30 October 2016 Norcia mainshock: the same records considered in previous paragraphs.

Impulsive forces due to seismic jerk are distinct from inertial forces due to acceleration. The former are generated by the variation of acceleration and may be much higher than the latter. Their influence on a structure depends on the frequency content of the jerk and the dynamic properties of the structure itself.

The integral of jerk is, by its own definition, an acceleration. Since acceleration, according to Newton's Second Law, is force per unit mass, the definite integral of jerk in the interval between two consecutive zeros may be referred to as "impulsive force per unit mass" (F_{imp}/m). Two consecutive zeros of jerk correspond to a maximum and a minimum of acceleration, or vice-versa. The signed area bounded by the jerk function in that interval corresponds to the impulse of acceleration or deceleration. Therefore, considering the interval between instants t_1 and t_2, the impulsive force per unit mass is given by:

$$\frac{F_{imp}}{m} = \int_{t_1}^{t_2} j(t)\, dt \tag{5}$$

This expression can be applied to any of the three jerk components, each one characterized by its own sequence of zeros.

Figure 20 illustrates the definition of impulsive force per unit mass as the area bounded by the jerk function $j(t)$ between two consecutive zeros. Yellow color indicates the positive impulsive force corresponding to an interval where acceleration increases: $a(t)$ goes from a minimum to a maximum. Instead, green color indicates the previous negative impulsive force corresponding to the interval where acceleration decreases going from a maximum to a minimum.

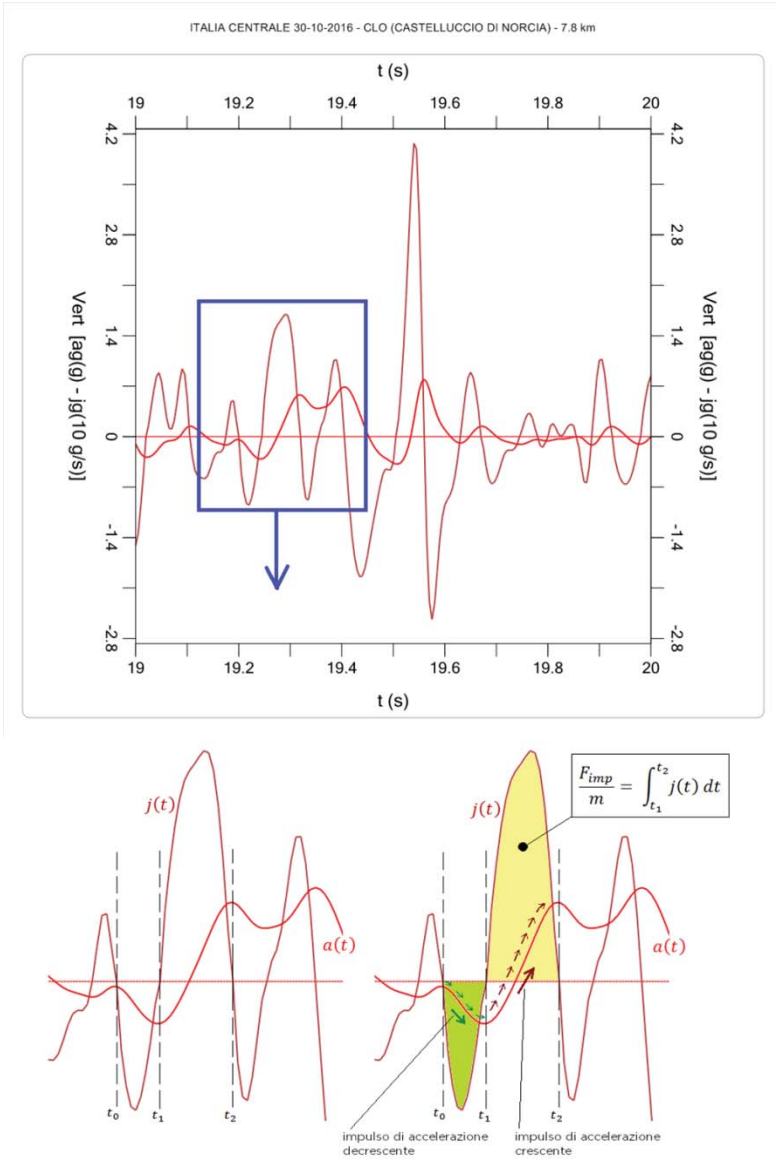

Figure 20. Impulsive force per unit mass, defined as the integral of jerk between two consecutive zeros

Figure 20 refers to the vertical component of the ground motion recorded at station CLO (Castelluccio di Norcia) from 30 October 2016 Norcia mainshock in the time interval (19.000 – 20.000 s).

It is worth noticing the very short duration of the impulsive forces. The considered jerk zeros correspond to the following instants in the record: t_0 = 19.200 s, t_1 = 19.245 s, t_2 = 19.320 s. The negative impulsive force corresponding to decreasing acceleration lasts 45 ms while the following positive impulsive force lasts 75 ms.

Thus, impulsive force may be calculated throughout the record for each time interval between two consecutive jerk zeros. The result is a step function that represents the time series of impulsive force per unit mass.

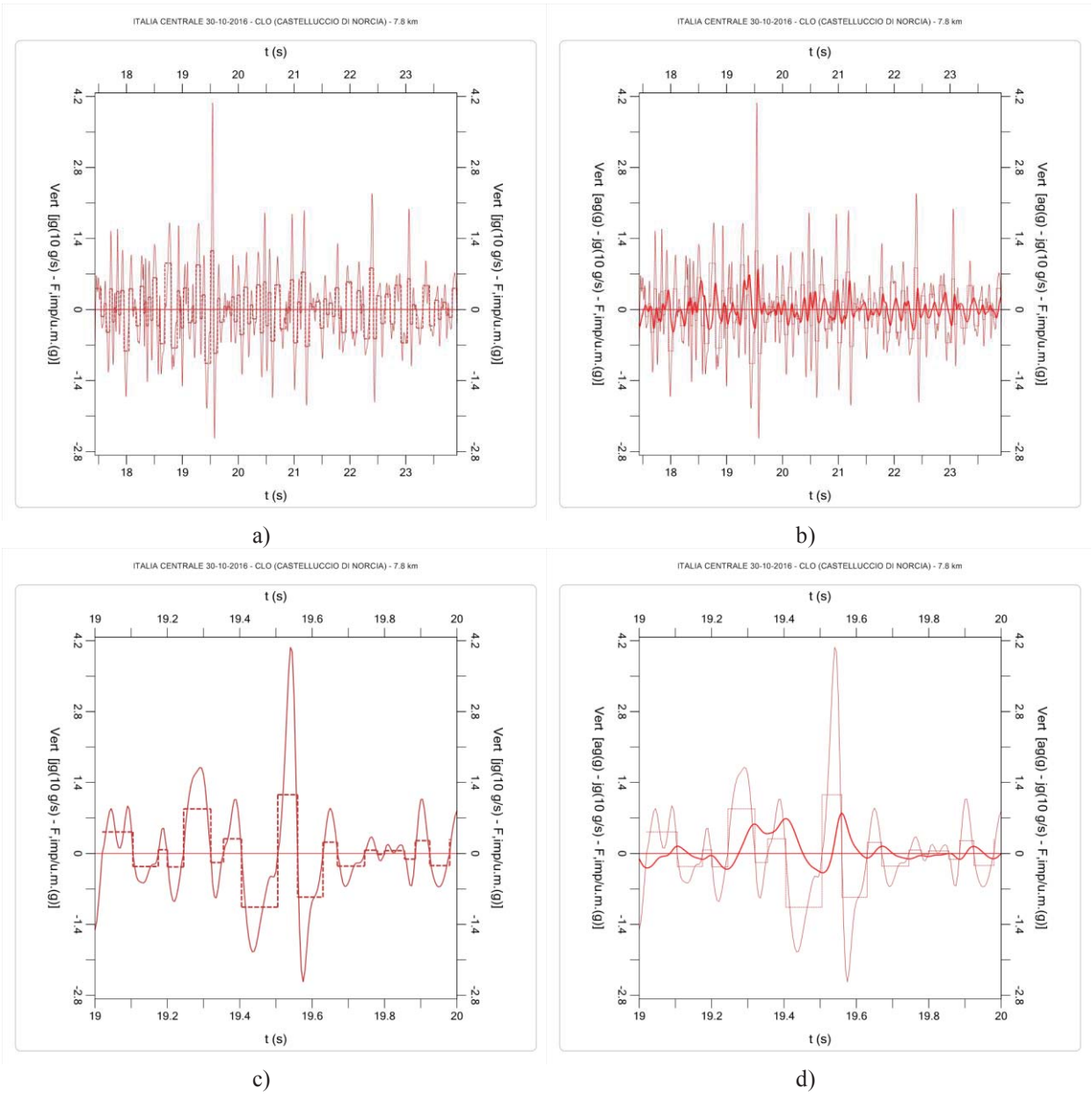

Figure 21. Jerk and impulsive forces per unit mass for the vertical seismic component. CLO - 30 October 2016 Norcia mainshock

Figure 21 shows jerk time series and step function of impulsive forces per unit mass (dashed line) for the vertical component of the reference seismic motion. The graphs on the right (b, d) also display the correspondent acceleration time series. The graphs at the top (a, b) refer to the time span between first and last acceleration peak exceeding 0.250 g, while the graphs at the bottom (c, d) refer to a shorter time interval (19.000 – 20.000 s).

The detail shown in Figure 22 highlights an important aspect: the value of the impulsive force cannot be directly correlated to the jerk level because it depends also on the time interval between two zeros. Therefore, lower jerk peaks with longer duration may yield higher impulsive forces than higher jerk peaks with shorter duration (cfr. Impulsive forces A and B in Figure 22).

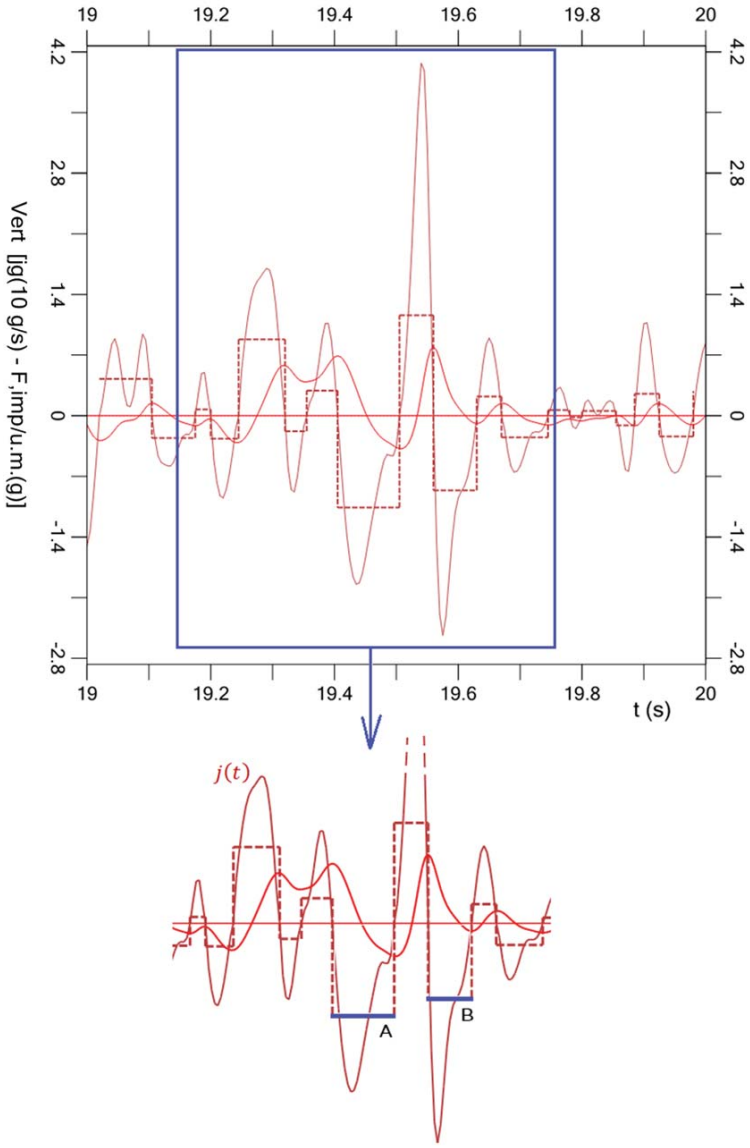

Figure 22. Peaks of jerk and correspondent impulsive forces

This behavior has general validity, it applies to all the components of seismic motion and different seismic events: the maximum values of jerk and impulsive force do not occur at the same time. The same happens between peaks of acceleration and peaks of jerk. Therefore, we get to the following property: PGA, PGJ and $F_{imp,max}$ are not simultaneous and there is not a direct relationship between them. This applies for any seismic event, any station, any of the three components of seismic motion.

Figures 23-25 show, for the reference seismic motion, the time series of impulsive force for each of the three components cut-off at the acceleration threshold of 0.250 g. The graphs on the left also include overlaid jerk time series (scale is uniform among the graphs on the left and among the graphs on the right).

Figure 26 shows the time series of the three components of impulsive forces overlaid in the same graph.

Thus, the dynamic nature of the seismic action is expressed, through jerk, by a series of consecutive impulses which determine vibrations; these are concept well known in Mechani-

cal Engineering, where forces induced by jerk are kept under control e.g. in order to optimize production processes [13].

Table 3 extends the information given in Table 2 with the maximum impulsive forces so to compare them with PGA and PGJ. Given their instantaneous nature and the independence between the three components, the impulsive forces are not combined in a unified 3D value. However, given the chaotic nature of the seismic motion, high values of impulsive force may occur simultaneously in different directions.

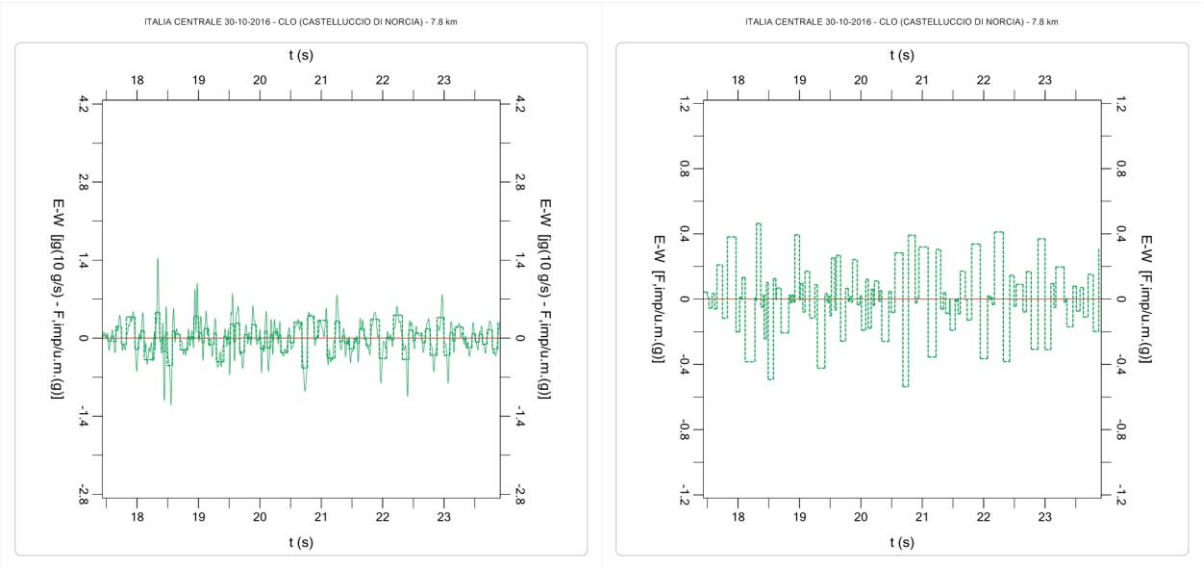

Figure 23. Jerk and impulsive force per unit mass: EW component

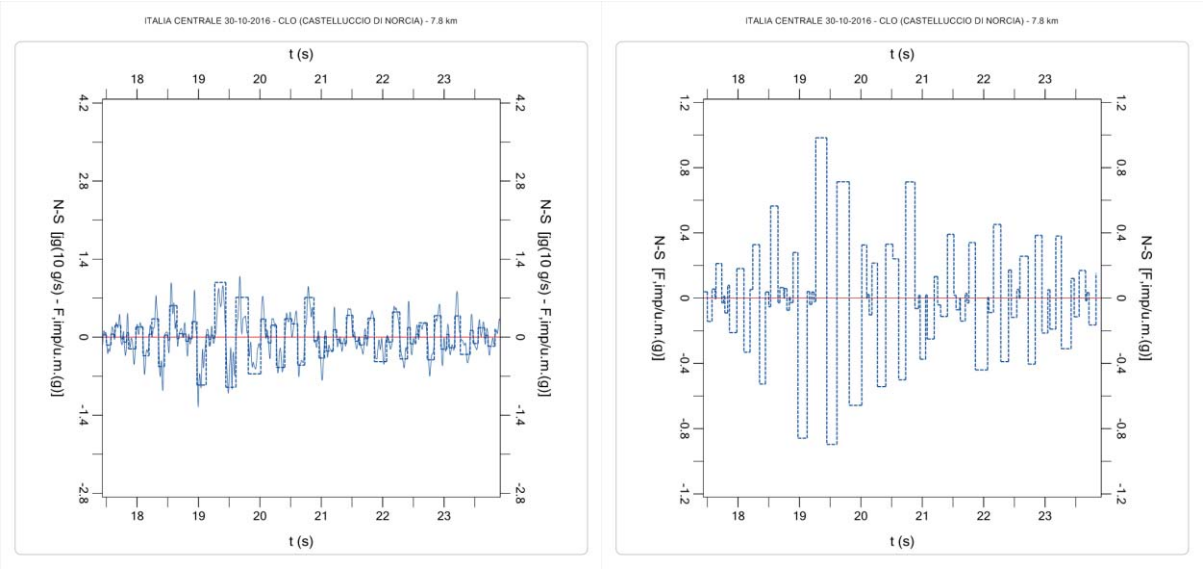

Figure 24. Jerk and impulsive force per unit mass: NS component

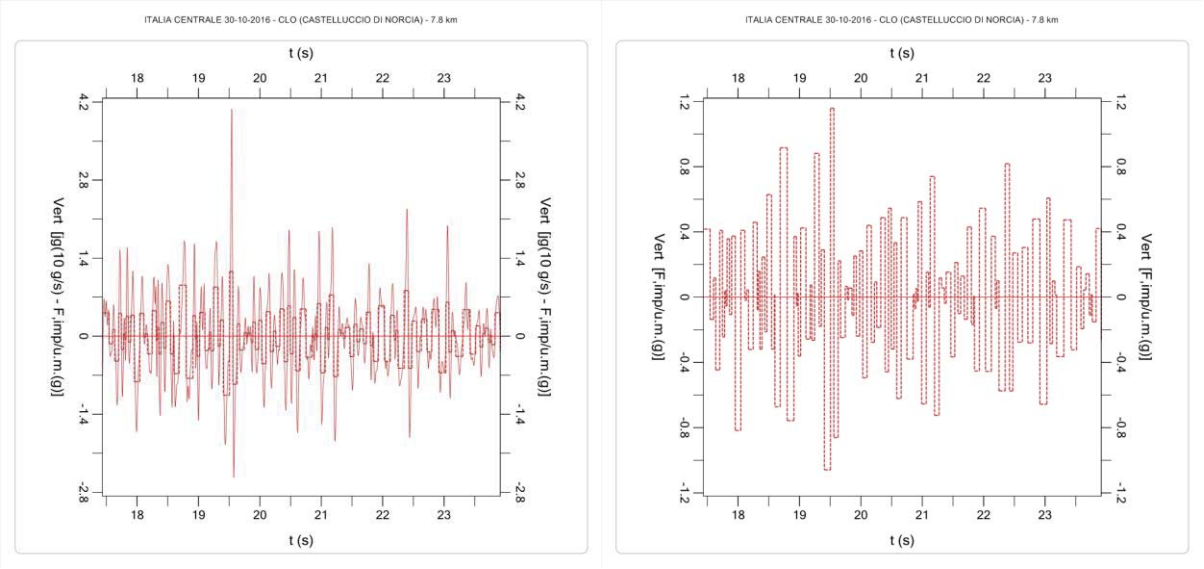

Figure 25. Jerk and impulsive force per unit mass: vertical component

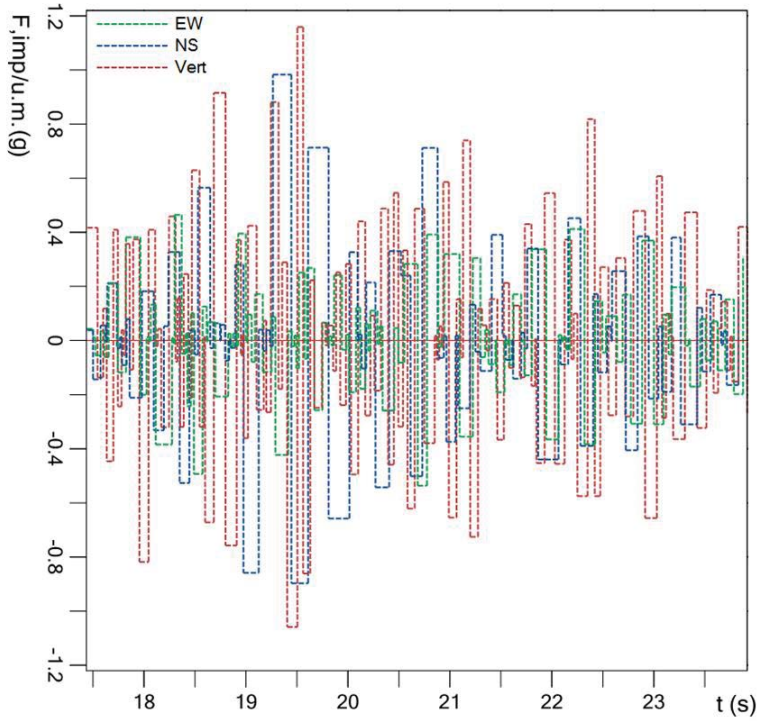

Figure 26. Time series of impulsive force per unit mass. All three components overlaid

Table 3 made clear how high the values of impulsive forces may be: for the reference seismic event (CLO, 30 October 2016 Norcia mainshock) the vertical impulsive force per unit mass exceeds gravity and reaches 1.159 g.

This means that during the seismic event there was a short time interval (55 ms, 19.505 s – 19.560 s) where the vertical "jolt" induced a force which exceeded weight (force of gravity) by more than 15%. Structures were subject to very demanding dynamic stress causing damages and collapses which cannot be fully understood if the analysis considers only the inertial forces due to ground acceleration.

Jerk thresholds significant for building damages need to be identified. Tong et Al. (2005) [11] highlighted that jerk larger than 2 g/s causes discomfort in people inside buildings. It is a threshold much higher (about 10 times higher) than criteria used by the transportation industry to ensure passenger comfort (about 0.2 g/s). The threshold of 10 g/s is the one within which structural damages may become severe.

Furthermore, the effects of jerk must be related to its frequency content: these aspects may be addressed through Fourier analysis.

	EW	t (s)	NS	t (s)	Vert.	t (s)	3D	t (s)
PGA (g)	0.427	20.775	0.583	19.445	0.797	19.560	0.829	19.410
PGJ (g/s)	14.36	18.335	12.50	18.995	40.70	19.540	41.69	19.540
$\frac{F_{imp,max}}{m}$ (g)	0.537	20.685 20.775 (**90** ms)	0.984	19.265 19.445 (**180** ms)	1.159	19.505 19.560 (**55** ms)		

Table 3. Peaks of acceleration, jerk and impulsive force per unit mass. Station CLO, 2016 Norcia mainshock

4 FREQUENCY ANALYSIS

The frequency content of a time series is expressed by the Fourier amplitude spectrum. Identification of the dominant frequency of the seismic motion is crucial for the comparison with the fundamental frequency of the structures.

Tong et al. (2005) [11], in their study on the 1999 Chi-Chi earthquake in Taiwan, provided Fourier amplitude spectra both for acceleration and jerk. The dominant frequency contents of the acceleration and jerk time series are between 1 and 10 Hz; however, jerk distributes in a much wider frequency band and its higher frequency contents are prominent.

This characteristic, observed for the first time in this seismic event in Taiwan, is confirmed for all seismic events in the Italian territory elaborated in this work. The jerk Fourier spectrum features a window of dominant frequency wider than the acceleration one. The jerk higher frequency content appears more important.

A parameter that characterized the frequency content is the mean period T_m, defined as the average of periods in the Fourier spectrum, each weighted by the square of its Fourier amplitude (Rathje et al. [14])

While the mean period of acceleration is generally quite large with values even higher than 1 s, the mean period of jerk is much lower with values comparable to typical fundamental periods of buildings.

Fourier analysis has been performed on the seismic records from station CLO (Castelluccio di Norcia) for 30 October 2016 Norcia earthquake. Figures 27-29 show the Fourier amplitude spectra of acceleration and jerk with the indication of the mean period for the three components of the seismic motion (EW, NS, Vert.).

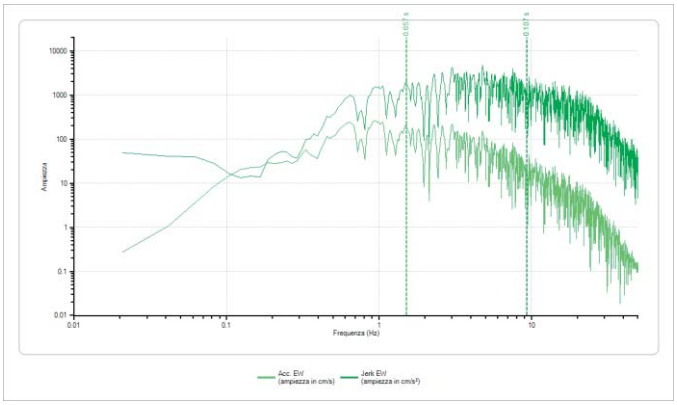

Figure 27. CLO, 2016 Norcia earthquake:
acceleration and jerk Fourier amplitude spectra for EW component

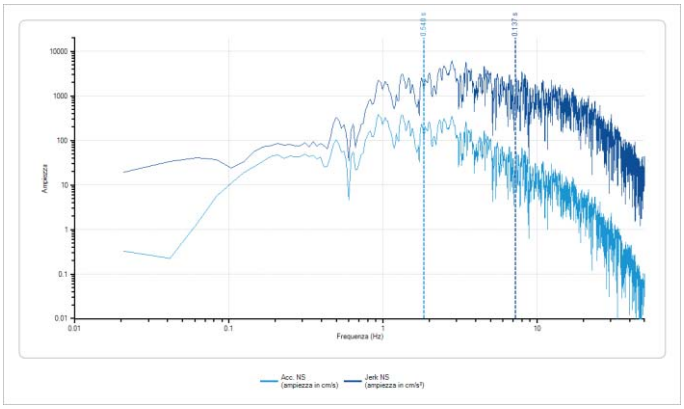

Figure 28. CLO, 2016 Norcia earthquake:
acceleration and jerk Fourier amplitude spectra for NS component

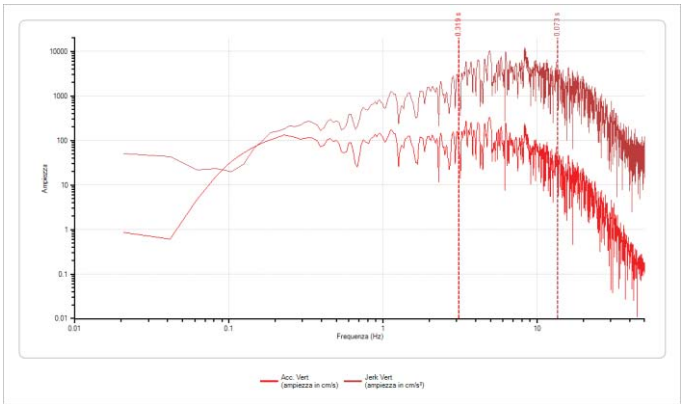

Figure 29. CLO, 2016 Norcia earthquake:
acceleration and jerk Fourier amplitude spectra for vertical component

T_m(s)	EW	NS	Vert.
Acceleration	0.657	0.540	0.319
Jerk	0.107	0.137	0.073

Table 4. Mean period of acceleration and jerk. CLO, 2016 Norcia earthquake

Table 4 highlights an important aspect: the main frequencies of the vertical component are significantly higher than the horizontal ones. This is also evident by the overlaid three-components Fourier spectra shown in Figures 30-31 for acceleration and jerk respectively. The jerk mean periods appear very close to fundamental periods of rigid structures like masonry buildings. This points out the prospect of critical issues caused by impulsive action on structural elements.

Records from CLO station for 30 October 2016 Norcia earthquake have been taken as reference for the elaborations presented so far, but the highlighted observation can be generalized and deepened through the analysis of a larger number of records.

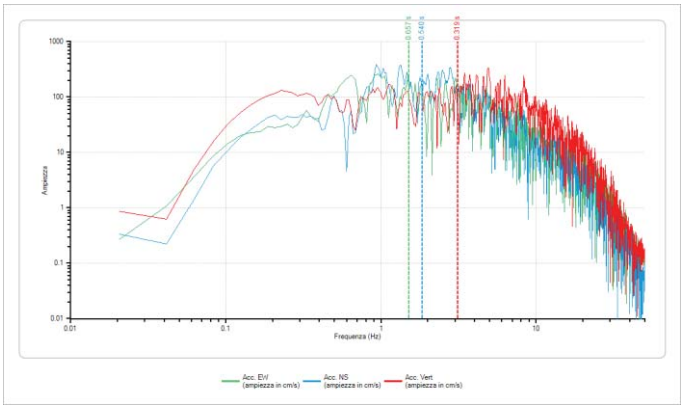

Figure 30. CLO, 2016 Norcia earthquake:
overlaid Fourier spectra for the three components of acceleration

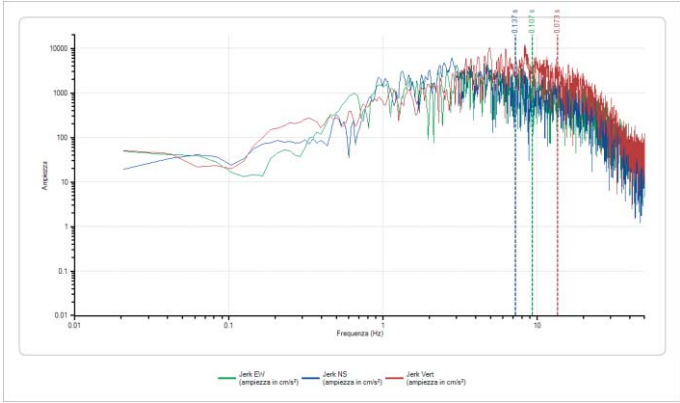

Figure 31. CLO, 2016 Norcia earthquake:
overlaid Fourier spectra for the three components of jerk

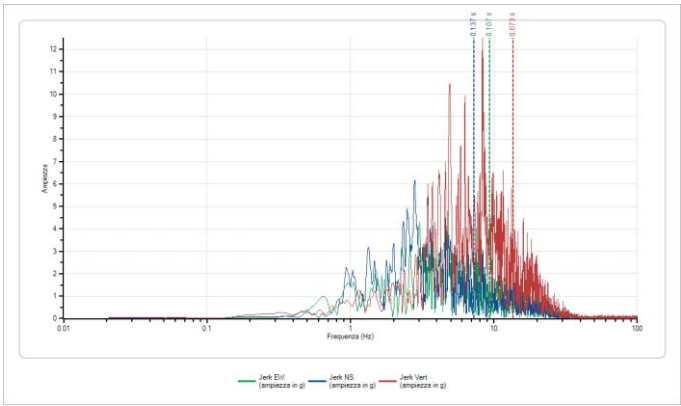

Figure 32. CLO, 2016 Norcia earthquake:
overlaid Fourier spectra for the three components of jerk
(logarithmic scale for frequency, natural scale for amplitude)

5 SEISMIC EVENTS ON ITALIAN TERRITORY: ELABORATIONS AND ANALYSES

The following study is based on ground motion records provided by ITACA project [12] for 8 reference seismic events: 30 October 2016 Norcia; 24 August 2016 Accumuli; 29 May 2012 Emilia; 6 April 2009 L'Aquila; 26 September 1997 Umbria-Marche; 23 November 1980 Irpinia; 19 September 1979 Valnerina; 6 May 1976 Friuli.

ITACA database provides records of these events taken from numerous stations. The signals are already corrected, thus, can be directly elaborated for the purposes of this work.

The performed elaborations highlighted some common aspects:

- the farer is the station from the epicenter, the shorter is jerk duration and the lower is its peak value.
- the farer is the epicenter the lower are the impulsive forces per unit mass; however, they remain higher than peak ground acceleration.
- the mean period of the vertical jerk component is always significantly lower than the horizontal components. Jerk represents the impulsive content of the seismic motion which is enhanced in the vertical component.
- stations farer form epicenter show attenuation of impulsive content through jerk drop. Vertical jerk component attenuates with respect to other horizontal components.

As an example, Table 5 reports the results for three stations recording 30 October 2016 Norcia mainshock.

Through statistical elaboration of the records, trend lines correlating PGA, PGJ and Impulsive Forces may be outlined.

This constitutes the first step for considering impulsive forces in structural design. If ground jerk and correspondent impulsive forces are not known, an estimation is required in order to evaluate their effects on structures.

30 October 2016 Norcia earthquake. Station and epicentral distance ➔	1_1 - CLO Castelluccio di Norcia, 7.8 km	1_2 - ACC Accumuli 18.6 km	1_3 - FBR Fabriano 59.1 km
Acceleration, Jerk and Impulsive Force per unit mass			
$\Delta t(j_g \geq 2.0$ g/s)	31.440 (16.410 - 47.850)	13.750 (7.395 - 21.145)	7.905 (17.465 - 25.370)
EW: PGA	0.427	0.434	0.079
PGJ	14.36	18.25	5.39
F_{imp} max	0.537	0.744	0.155
NS: PGA	0.583	0.392	0.066
PGJ	12.50	12.15	3.46
F_{imp} max	0.984	0.660	0.121
Vert.: PGA	0.797	0.558	0.049
PGJ	40.70	35.88	2.21
F_{imp} max	1.159	0.887	0.095
Mean period from Fourier amplitude spectra (T_m)			
EW: Acc.	0.657	0.397	0.234
Jerk	0.107	0.081	0.054
NS: Acc.	0.540	0.456	0.247
Jerk	0.137	0.083	0.060
Vert.: Acc.	0.319	0.179	0.232
Jerk	0.073	0.044	0.060

Seismic parameters and unit of measure:

$\Delta t(j_g \geq 2.0$ g/s)	(s)	Time span between first and last jerk peak exceeding 2.0 g/s
PGA	(g)	Peak ground acceleration
PGJ	(g/s)	Peak ground jerk
F_{imp} max	(g)	Maximum impulsive force per unit mass (based on jerk)
T_m	(s)	Mean period from Fourier amplitude spectra

Table 5. Acceleration and jerk and impulsive forces for 30 October 2016 Norcia earthquake

Among all the ground station records available for the 8 events considered, the ones taken into account in the statistical analysis were those with bracket duration of ground acceleration record longer than 100 ms when the threshold of 0.005 g is applied. In total 447 station records were considered. For each of them and for each of the three components (EW, NS, Vert.) the following parameters were elaborated by means of the software Seismic 3D:

1. peak ground acceleration (PGA)
2. peak ground jerk (PGJ)
3. maximum value of impulsive force per unit mass (F_{imp})
4. mean period (T_m) of acceleration and jerk from Fourier spectra

The statistical elaboration was performed separately for horizontal and vertical components. In the pursuit of useful correlation between the considered parameters, distinction between the two horizontal components (coming from different stations) appears inappropriate.

The correlations obtained between PGA, PGJ and F_{imp} are illustrated in Figures 33, 34, 35.

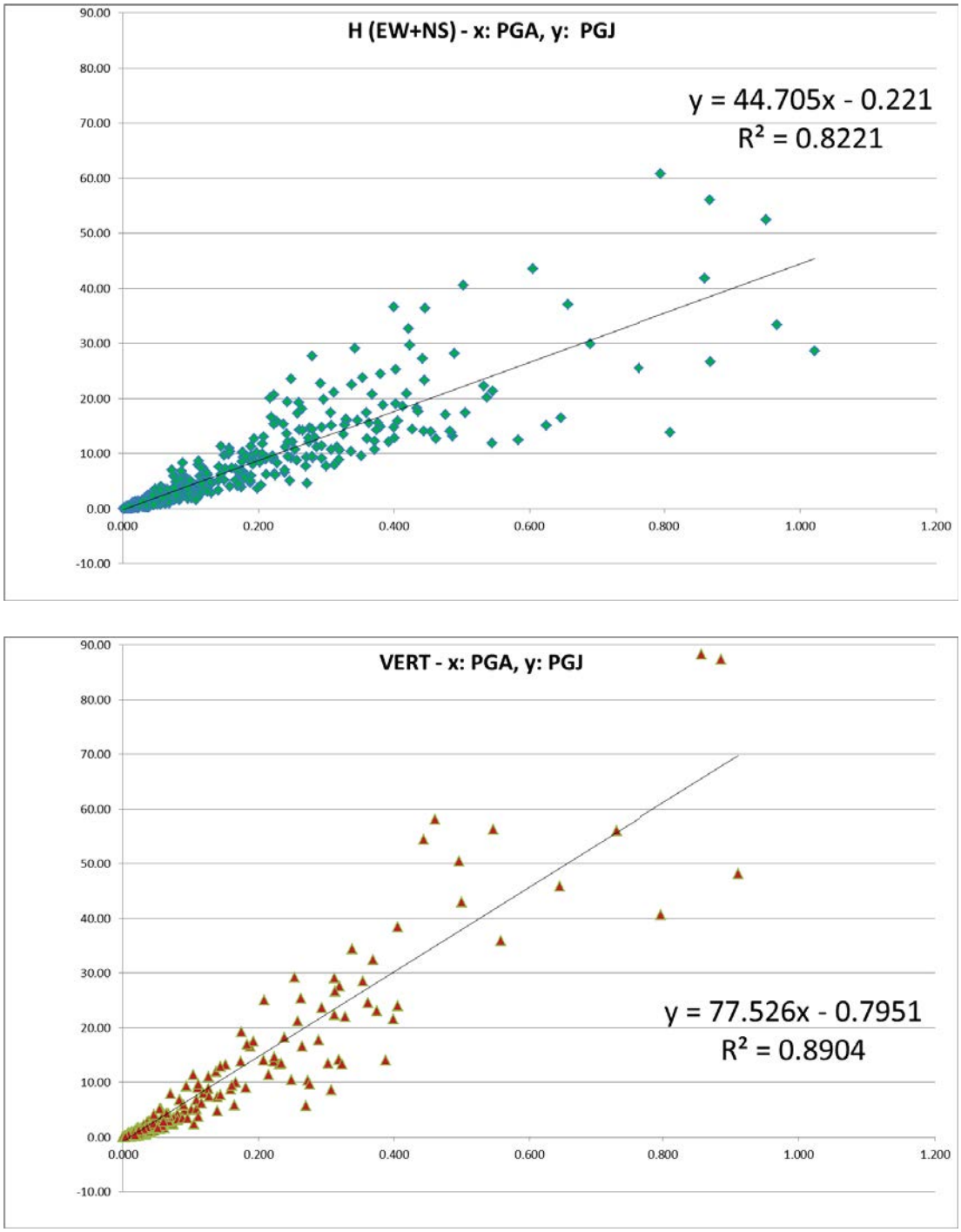

Figure 33. Correlation PGA-PGJ for horizontal and vertical components

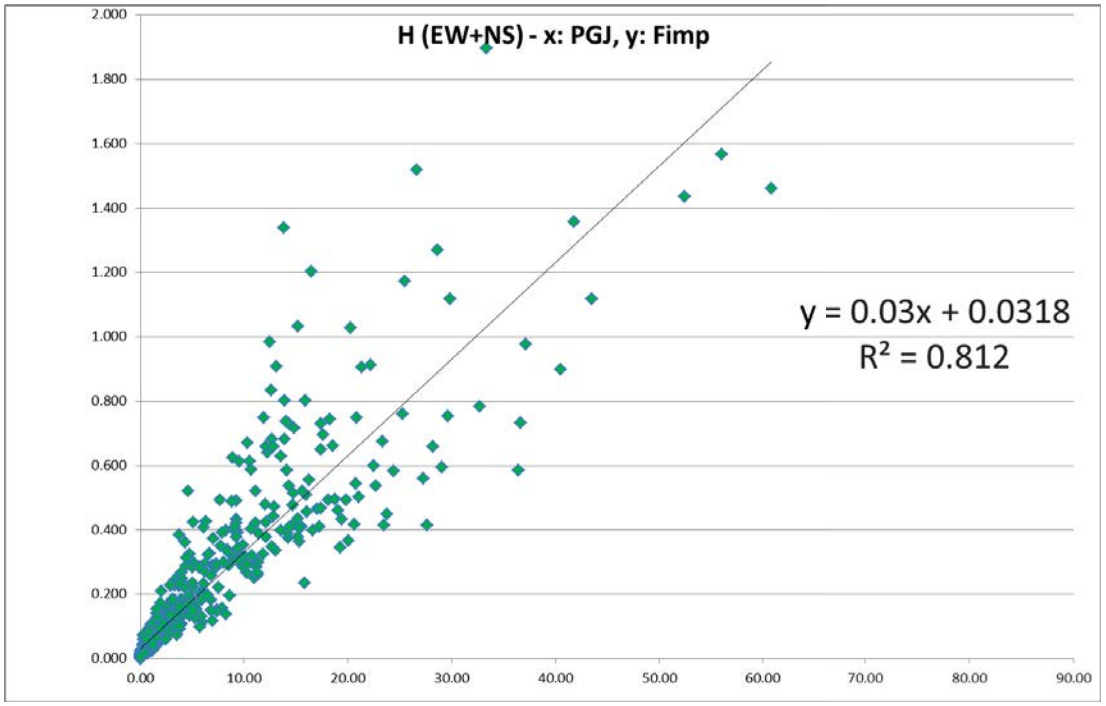

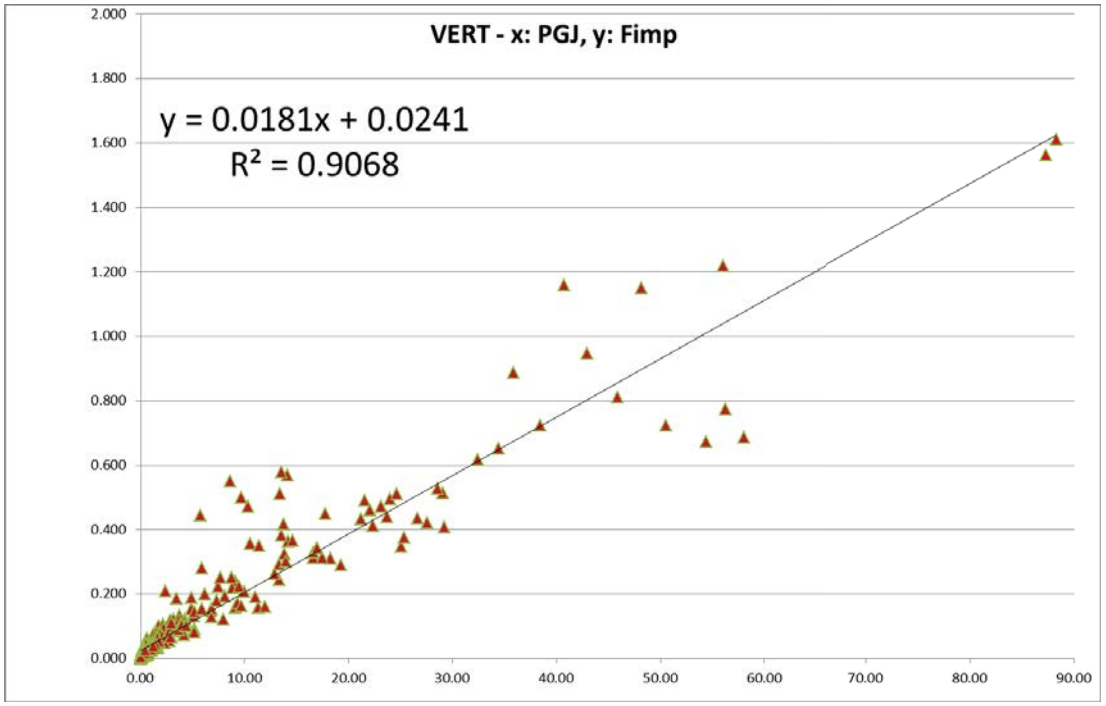

Figure 34. Correlation PGJ-Fimp determined through (5), for horizontal and vertical components

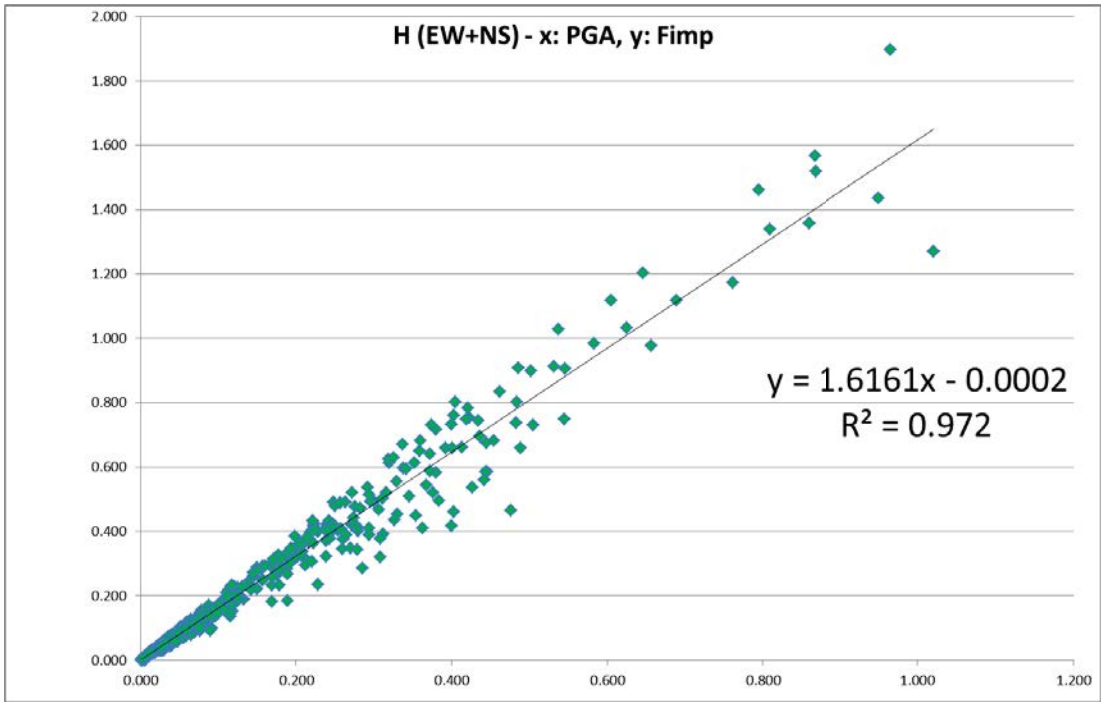

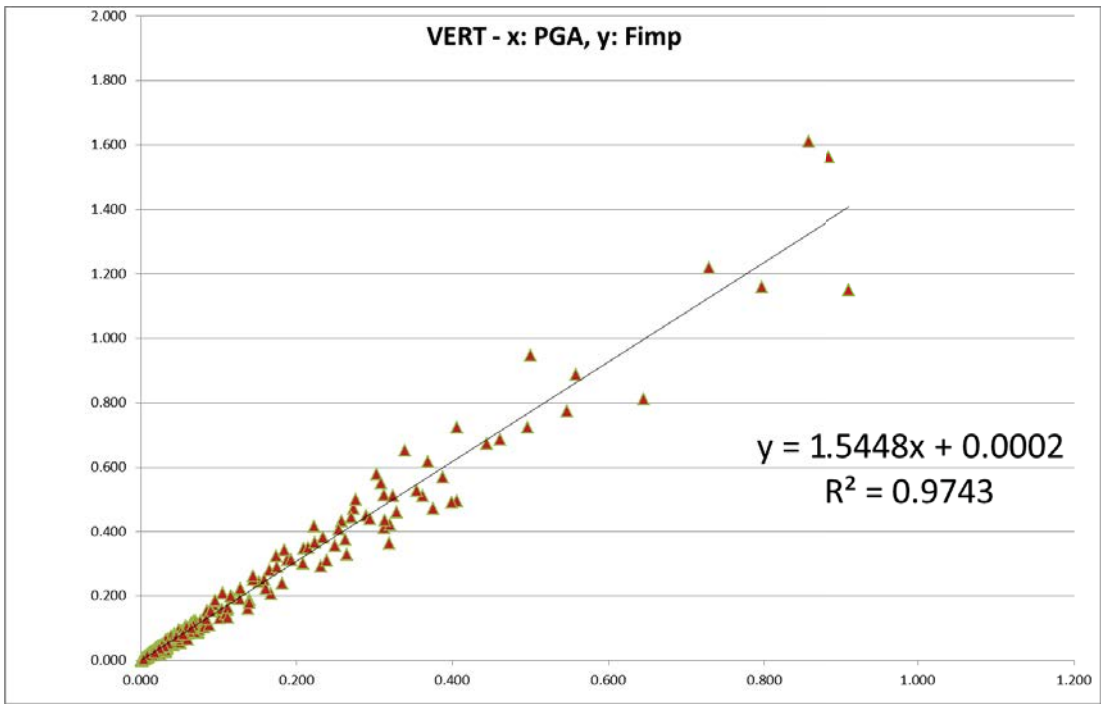

Figure 35. Correlation PGA-F_{imp} for horizontal and vertical components

The PGA-F_{imp} graphs show an excellent correlation: the relationship between peak ground acceleration and peak impulsive force is well described by the trend line.

Acceleration, jerk and impulsive force are generated by a chaotic phenomenon: the analytical operations carried out for determining jerk (through derivation of acceleration) or for calculating the impulsive forces are processes which do not correspond to a predefined analytical function.

The correlation between PGA and impulsive forces, obtained through elaboration of the main seismic events in Italy, is an intrinsic property of the events themselves. The fact that the cor-

relation has a coefficient of determination very close to 1 represents an excellent support for estimating the impulsive actions based on ground acceleration data.

The correlation obtained through statistical analysis between PGA (s) and PGJ (g/s) and between PGA (g) and maximum impulsive force per unit mass (g) are summed up in the following expressions (H stand for horizontal component, V stands for vertical component):

$$PGJ_H = 44.705\, PGA_H - 0.221 \quad (6)$$

$$PGJ_V = 77.526\, PGA_V - 0.795 \quad (7)$$

$$F_{imp,max,H} = 1.616\, PGA_H \quad (8)$$

$$F_{imp,max,V} = 1.545\, PGA_V \quad (9)$$

In order to validate the relationships determined through statistical analysis on Italian seismic events, we operate a comparison between the jerk values elaborated by Tong et al. [11] for the 1999 Chi-Chi earthquake in Taiwan and those calculated from PGA with expressions (6-7).

Station	Component	PGA (g)	PGJ (g/s) (Tong et Al.)	PGJ (g/s) (Mariani, Pugi)	PGJ delta vs Tong et Al.	F_{imp} (g)
CHY028	EW	0.630	21.50	27.94	30%	1.018
	NS	0.764	26.30	33.93	29%	1.235
	VERT	0.342	23.20	25.72	11%	0.529
TCU095	EW	0.378	13.80	16.68	21%	0.611
	NS	0.712	31.80	31.61	-1%	1.150
	VERT	0.255	19.80	18.97	-4%	0.394

Table 6. Comparison between the elaborations of Tong et Al. (2005) [11] and Mariani and Pugi (2020)

CHY028 station yields a difference of about 30% for the horizontal component. The difference is rather high, but it drops to 11% for the vertical component. Given the fact that the seismic event in Taiwan has no relation whatsoever with the Italian events and that the analytical procedure for calculating jerk (based on numerical differentiation) has been carried out independently, the result is satisfactory. Considering that the impulsive phenomenon is particularly associated to the vertical component, the value of 25.72 g/s estimated through (7) is in good agreement with the 23.20 g/s in Tong et Al. Moreover, these jerk values are rather high, definitely higher than the 10 g/s threshold considered the cause of important damages on buildings: the values of 25.72 and 23.20 g/s would result in similar effects induced on the structures.

A surprisingly high agreement is obtained for TCU095 station where the peak ground jerk for the NS component is practically coincident with the value calculated through (7): 31.61 vs. 31.80 (g/s). Also, the vertical jerk component is very close: 18.97 vs 19.80 g/s.

The statistical investigation carried out on jerk should be completed with the analysis of the frequency content. In fact, the effects of seismic motion depend on the way they are filtered by the structures: a reliable model for the evaluation of jerk impulsive action effects on structures requires a frequency analysis which could be carried out through the study of the mean period from Fourier amplitude spectra.

The definition of a statistical value of the mean period T_m would provide a realistic estimation of the main frequencies of acceleration and jerk.

The mean period T_m calculated from Fourier spectra has no relations with peak ground acceleration, peak ground jerk or maximum impulsive forces. Therefore, the investigation on the mean periods is carried out comparing directly the T_m values of the 447 station records considered. Some stations yielded T_m values significantly far from average due to local site effects. Since the scope of the analysis is the pursuit of a T_m value which could be representative of acceleration and jerk for generic events, it is preferable to associate it to the median value rather than the mean. The median value is less influenced by extremely large or small values and gives a better idea of which is the "typical" value.

Figures 36-41 report for the three components of acceleration and jerk the following information:

- the mean period T_m for each station considered. The graphs also show the mean value (black line) and the median value (red line) which in all the cases is lower than the mean.
- the frequency distribution with discretization of the periods in intervals of 0.1 s for acceleration and 0.025 s for jerk

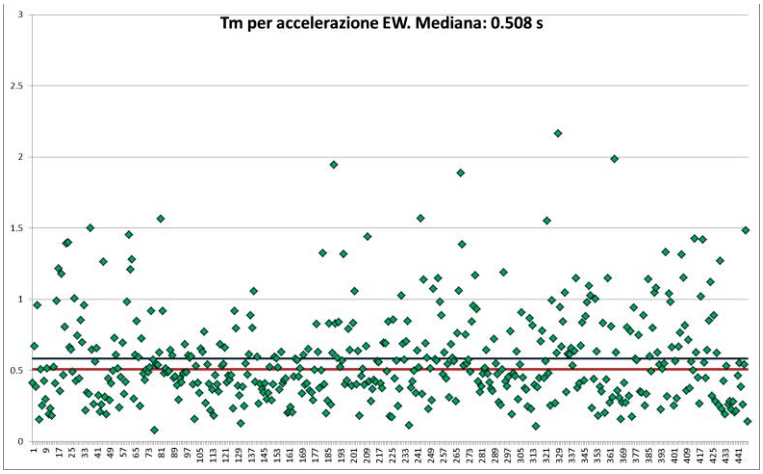

Classe	Frequenza	
0.1	0.22%	1
0.2	4.25%	19
0.3	12.75%	57
0.4	13.20%	59
0.5	18.79%	84
0.6	14.54%	65
0.7	11.41%	51
0.8	4.47%	20
0.9	5.82%	26
1	3.58%	16
1.1	3.13%	14
1.2	2.24%	10
1.3	1.12%	5
1.4	1.57%	7
1.5	1.34%	6
Altro	1.57%	7

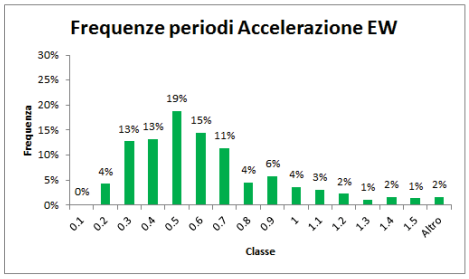

Figure 36. Statistical elaboration on the mean period T_m of acceleration EW component

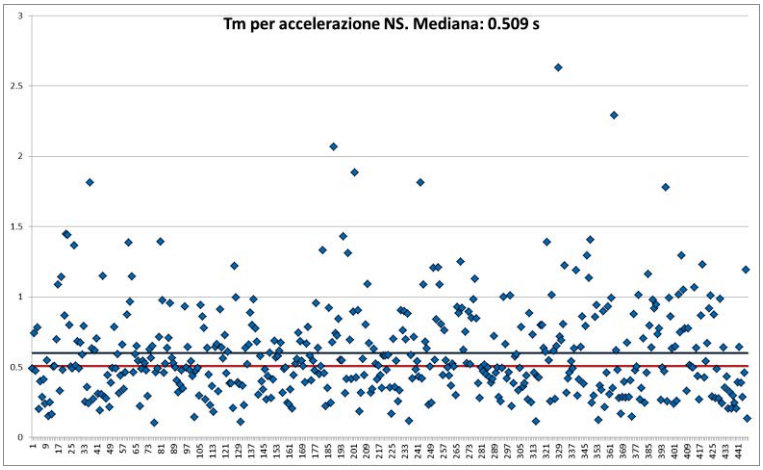

Classe	Frequenza	
0.1	0.00%	0
0.2	3.36%	15
0.3	13.65%	61
0.4	11.86%	53
0.5	18.79%	84
0.6	12.30%	55
0.7	11.63%	52
0.8	7.38%	33
0.9	5.59%	25
1	5.59%	25
1.1	2.46%	11
1.2	1.79%	8
1.3	1.79%	8
1.4	1.34%	6
1.5	0.89%	4
Altro	1.57%	7

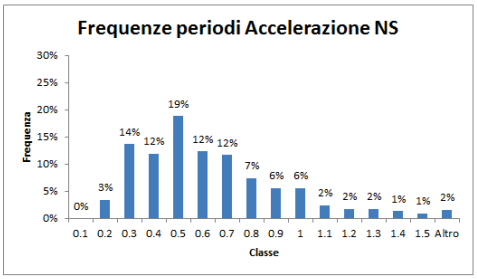

Figure 37. Statistical elaboration on the mean period T_m of acceleration NS component

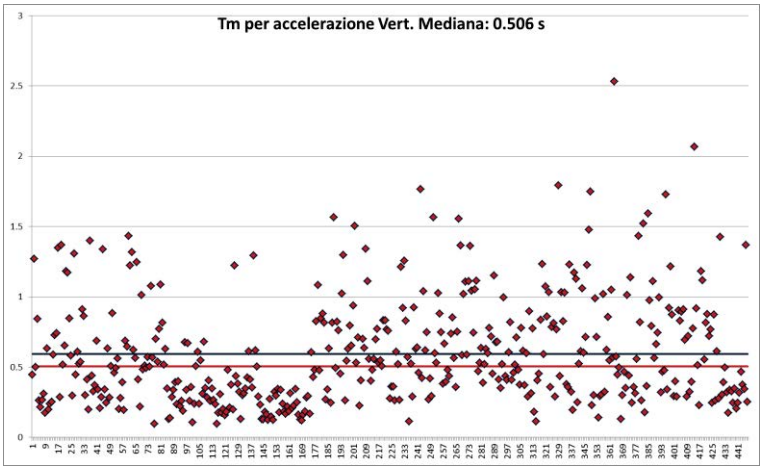

Classe	Frequenza	
0.1	0.45%	2
0.2	8.95%	40
0.3	15.21%	68
0.4	14.32%	64
0.5	10.29%	46
0.6	10.51%	47
0.7	8.95%	40
0.8	6.49%	29
0.9	6.71%	30
1	2.68%	12
1.1	4.03%	18
1.2	2.91%	13
1.3	2.68%	12
1.4	2.24%	10
1.5	0.89%	4
Altro	2.68%	12

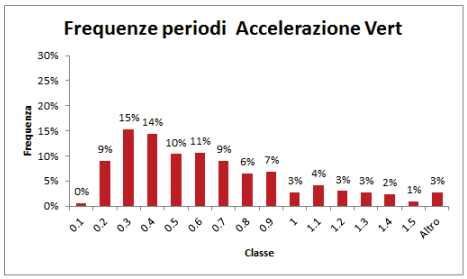

Figure 38. Statistical elaboration on the mean period T_m of acceleration vertical component

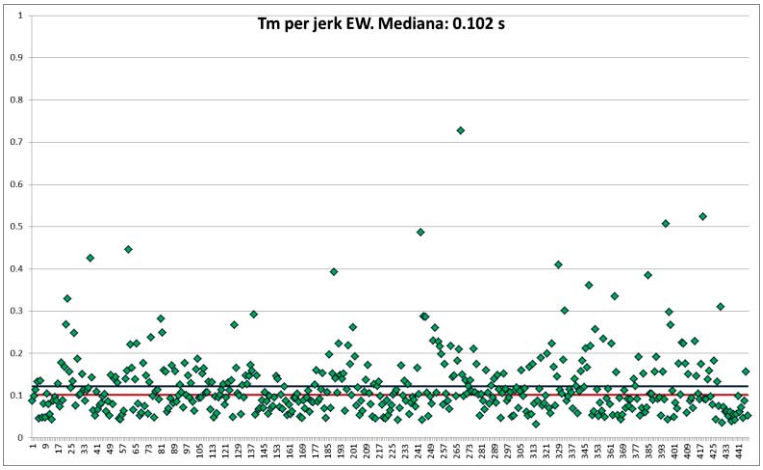

Classe	Frequenza	
0.025	0.00%	0
0.05	6.71%	30
0.075	19.46%	87
0.1	22.60%	101
0.125	16.78%	75
0.15	10.96%	49
0.175	9.17%	41
0.2	4.03%	18
0.225	2.91%	13
0.25	1.79%	8
0.275	1.34%	6
0.3	1.12%	5
Altro	3.13%	14

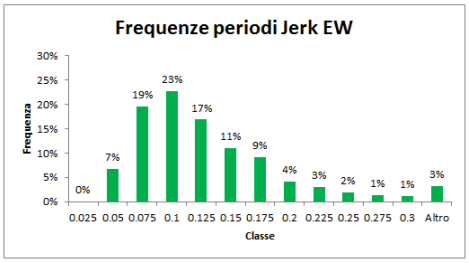

Figure 39. Statistical elaboration on the mean period T_m of jerk EW component

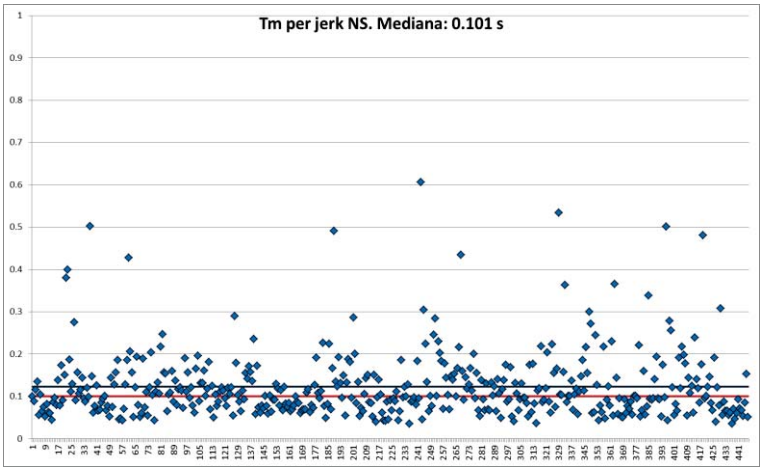

Classe	Frequenza	
0.025	0.00%	0
0.05	5.37%	24
0.075	21.25%	95
0.1	22.15%	99
0.125	17.45%	78
0.15	10.29%	46
0.175	7.38%	33
0.2	5.59%	25
0.225	3.58%	16
0.25	1.79%	8
0.275	0.45%	2
0.3	1.34%	6
Altro	3.36%	15

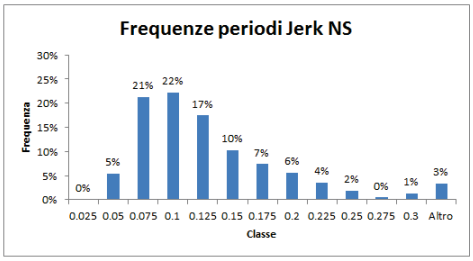

Figure 40. Statistical elaboration on the mean period T_m of jerk NS component

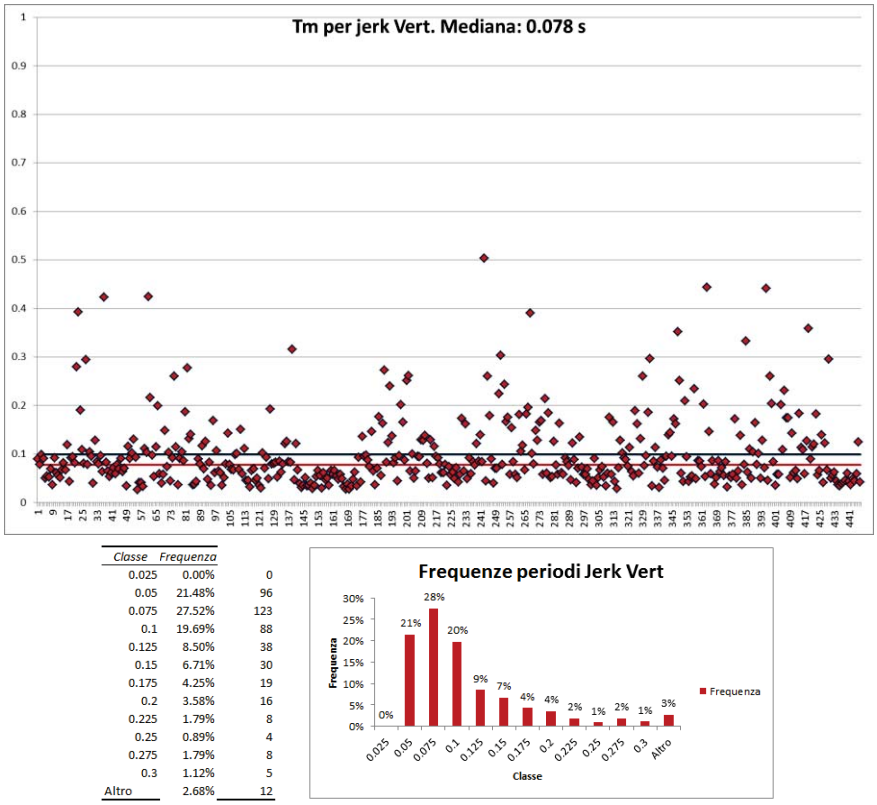

Figure 41. Statistical elaboration on the mean period T_m of jerk vertical component

Table 7 sums up the representative values of the mean periods and the main contribution to the distribution.

	T_m (s) and main contribution to the distribution	
Component	Acceleration	Jerk
EW	0.508 (19% for 0.500)	0.102 (23% for 0.100)
NS	0.509 (19% for 0.500)	0.101 (22% for 0.100)
Vert.	0.506 (15% for 0.300)	0.078 (28% for 0.075)

Table 7. Representative T_m for acceleration and jerk

From the analysis of the Fourier spectra it is evident that the main jerk frequencies are much higher than the acceleration ones. This aspect was already clear by the comparison of the Fourier spectra elaborated for Castelluccio di Norcia records of 2016 Norcia earthquake (Figures 27-29). This highlights the very nature of jerk which can be associated to the impulsive content of acceleration.

Moreover, while for acceleration there are not significant differences among the horizontal and vertical components, all characterized by $T_m \cong 0.500$ s, for jerk the difference is substantial ($T_m \cong 0.100$ s for horizontal components and $T_m \cong 0.075$ s for the vertical).

Therefore, jerk consists of higher frequency than acceleration and the vertical component accentuate this characteristic with respect to the horizontal components.

Jerk vertical component is particularly important since it represents the most impulsive content of seismic motion.

The conception that buildings, being designed to resist vertical loading, can undergo impulsive seismic action without damages while they suffer only the horizontal seismic action effects, is definitely overcome.

Moreover, in lights of the study on jerk, the negative effects of the vertical seismic component involve failures triggered by the rapid alternation of compression and decompression induced by vertical vibrations.

The seismic motion is a dynamic phenomenon; thus, the structural response is totally different from that under static loading.

Where the main frequencies of the seismic motion are close to the fundamental frequencies of buildings, seismic effects undergo maximum amplification and structural elements are subject to the most demanding actions.

Studying the different building typologies one can identify the cases where jerk effects may be critical and potentially cause damages: e.g., the fact that jerk mean periods are close to fundamental periods of masonry buildings suggests to investigate the link between impulsive forces and local damages such as masonry disaggregation and connection failures.

6 EFFECTS OF IMPULSIVE ACTIONS ON BUILDINGS

During this research, the few available studies on the variation of seismic acceleration were collected. Based on the various considerations of the authors and the results of this work, the following 7 aspects may be highlighted:

1) Inertial force induced by acceleration and impulsive action due to variation of acceleration are two complementary aspects: both should be considered when assessing the structural behavior (Tong et Al. [11]);
2) During 1999 Chi-Chi earthquake acceleration records obtained from sensor placed at different levels of seven-story RC building showed that jerk amplification is substantially similar to that of acceleration (Tong et Al. [11]);
3) The attenuation of the Jerk design response spectrum with respect to the elastic spectrum is lower than what occur for acceleration. For low periods (rigid structures) the impact reduction factor R_J is practically equal to 1, so the jerk design response spectrum is almost coincident with the elastic one (Haoxiang He et Al. [15]).
4) In general, improving ductility jerk effect will reduce, that is, the impact reduction factor R_J increases, in a manner similar to the behavior factor q for acceleration spectra (Haoxiang He et Al. [15]). For the horizontal components of the seismic motion, useful information for design purposes are given by the jerk response spectra illustrated in Figures 42-43 (Haoxiang He et Al. [15]).
5) The propagation of jerk vibrational waves is directly related to stress concentration and local damages, which in homogeneous material are initiated by molecular bond separation (Y. Xueshan et Al. [16]). In the case of masonry, it comes naturally to extend this concept to the macroscopic level of stones separation for mortar disaggregation.
6) In existing masonry buildings, strengthening interventions aimed at confining the structural elements prevent local concentration of stresses and improve the response with respect to jerk (Sofronie [17-18]). Considering the short duration of the impulsive action and the rigid-brittle behavior of masonry, such interventions may be verified in terms of resistance. In general, in existing masonry buildings, it is crucial to ensure resistance with respect to local damages such as masonry disaggregation and failure of connections between different structural elements.

7) The effects of jerk are particularly important in vertical direction. In fact, the vertical components are more impulsive than the horizontal ones, as described by the lower mean period in Fourier spectra (Table 7).

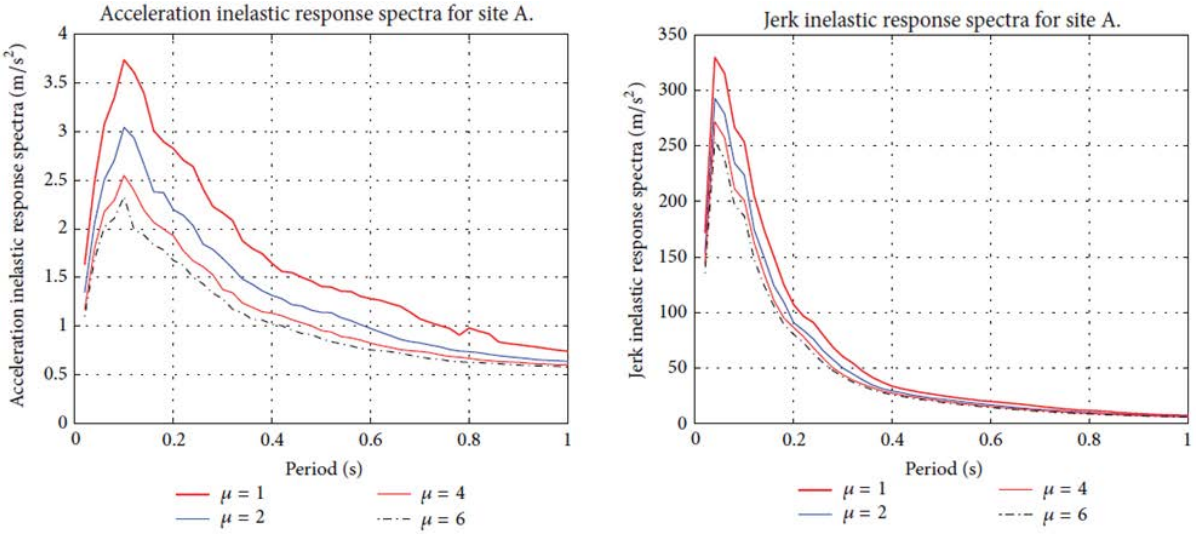

Figure 42. Acceleration and jerk inelastic response spectra for site A.
Statistical elaboration by Haoxiang He et Al. [15]

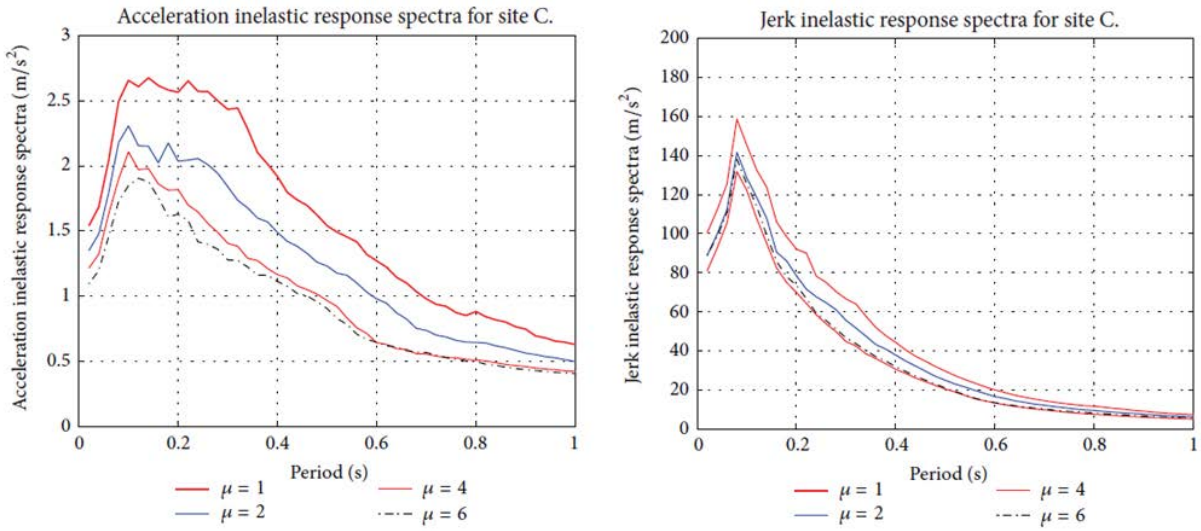

Figure 43. Acceleration and jerk inelastic response spectra for site C.
Statistical elaboration by Haoxiang He et Al. *[15]*

In light of the correlation between seismic jerk and physical damage of materials and structural elements during a seismic event, some considerations on seismic monitoring activity should be made.

At the moment, drift ratio, that is the relative displacement between two floors divided by the vertical distance between them, is the main parametric indicator of damage condition in a monitored building [19].

This parameter is monitored through software processing real-time measurements of displacements acquired through double integration of accelerometer time-series data. Other mon-

itored parameter are the periods of vibration, the peak ground acceleration (PGA) and peak structure acceleration (PSA), but only in the two horizontal direction X and Y.

Drift ratio is truly representative of damage condition in framed steel or RC structures; but in masonry structures, very rigid and strongly characterized by brittle types of failures, this parameter appears less consistent with respect to jerk monitoring.

The difference between the two parameters is also the possibility to represent through jerk the spatial effects of seismic motion, including the vertical component: drift ratio completely disregards this aspect.

Furthermore, jerk monitoring may provide important information on the assessment of local failures in other structural typologies: e.g. joint failures in steel frames [20, 21].

Given the relation between high values of impulsive forces and damage in areas with high stress concentration, the maximum values of jerk (PGJ and PSJ) play a significant role in the assessment of the negative effects induced by the seismic motion.

Placement of triaxial jerk sensor, available for some years now [16], or the real-time analytical calculation of jerk time series, may further enhance the quality of the monitored information with clear benefits on the quick definition of the damage scenarios, one of the main objectives of seismic monitoring.

The negative effects of the vertical jerk component are highlighted by the impulsive nature of the phenomenon and the high vertical stiffness of the structure. Therefore, amplification effects due to high similarity between fundamental period of the structures and jerk mean period should be investigated.

Jerk is characterized by high frequencies. The statistical analysis on the main recent seismic events in Italy found that the representative mean period of the vertical jerk component is about 0.075 s, which is very close to the fundamental period of vertical vibration of many rigid structures, such as masonry buildings.

To be more specific about the amplification of the structural response in terms of displacements and internal actions, considering that seismic input is a combination of many harmonic excitations, we can refer to the theory of driven harmonic oscillators with viscous damping.

Study of the simple oscillator leads to an amplification factor C_{ampl} given in expression (10):

$$C_{ampl} = \frac{1}{\sqrt{\left(1 - \frac{T_1^2}{T^2}\right) + 4\,\xi_{eq}^2\,\frac{T_1^2}{T^2}}} \tag{10}$$

where: T_1 is the fundamental period of the structure; T is the period of the applied force (in this case coincident with the mean period of vertical jerk component); ξ_{eq} is the equivalent viscous damping coefficient.

By applying (10) we get that with a period of the applied force T = 0.075 s, the vertical impulsive effect is amplified for fundamental periods T_1 in the range [0 - 0.105 s] with maximum amplifications for T_1 in the range [0.050 s – 0.090 s].

With T = 0.050 s, the amplification is obtained for T_1 in the range [0 - 0.070 s] with maximum amplifications for T_1 in the range [0.040 s – 0.060 s].

With T = 0.050 s, the amplification is obtained for T_1 in the range [0 - 0.140 s] with maximum amplifications for T_1 in the range [0.075 s – 0.120 s].

In all the examined cases, amplification occurs for ranges of vertical fundamental periods T_1 which include those of a wide class of masonry buildings. This aspect is crucial for determining the vertical impulsive actions along the building elevation and their effects on the structural elements.

Moreover, the structural effects of the impulsive actions are also affected by jerk variation, that is, the time derivative of jerk referred to as snap [21-22]. We can imagine that the variation of acceleration generates a "jolt" which in turn contains a series of smaller "jolts" related to higher-order derivatives. Snap can be represented in space as a vector with one component tangent to the acceleration path (thus parallel to jerk) and one orthogonal component associated to the change of direction. When the changes of direction are particularly important, strengthening elements able to resist "jolts" along different and suddenly variable directions should be designed. Therefore, the strengthening intervention should provide resistance distributed as much as possible.

7 CONSTRUCTION DETAILS FOR MASONRY ELEMENTS STRENGTHENING

In light of the findings of this research about the effects of impulsive actions on existing masonry buildings, two construction details of particular strengthening interventions are presented.

The interventions aim at enhancing the resistance of structural discontinuity regions, load application points, stress concentration areas, joints, etc., in agreement with current Technical Standards (Italian guidelines: CNR DT 214/2018 - Istruzioni per la valutazione della robustezza delle costruzioni, §6.1.1).

This work highlighted the importance of masonry confinement and improvement of connections between distinct structural elements, both in vertical and horizontal planes. The interventions aim at enhancing structure robustness through three-dimensional ties.

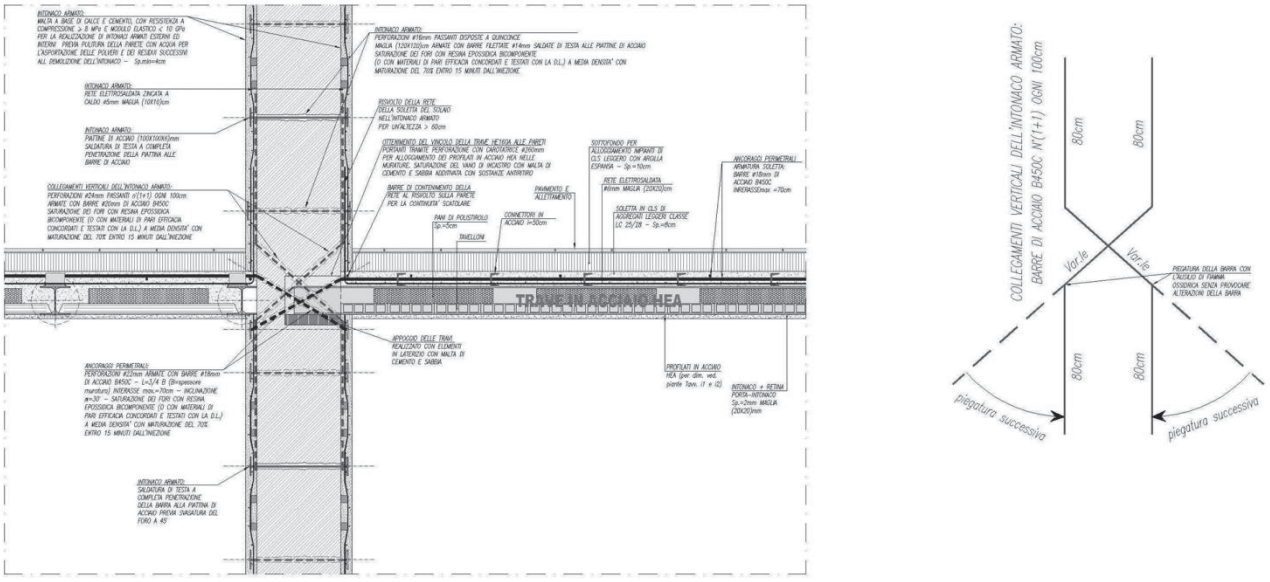

Figure 44. Vertical connection between reinforced mortar and internal masonry pier in correspondence of a steel slab (original drawings by Massimo Mariani)

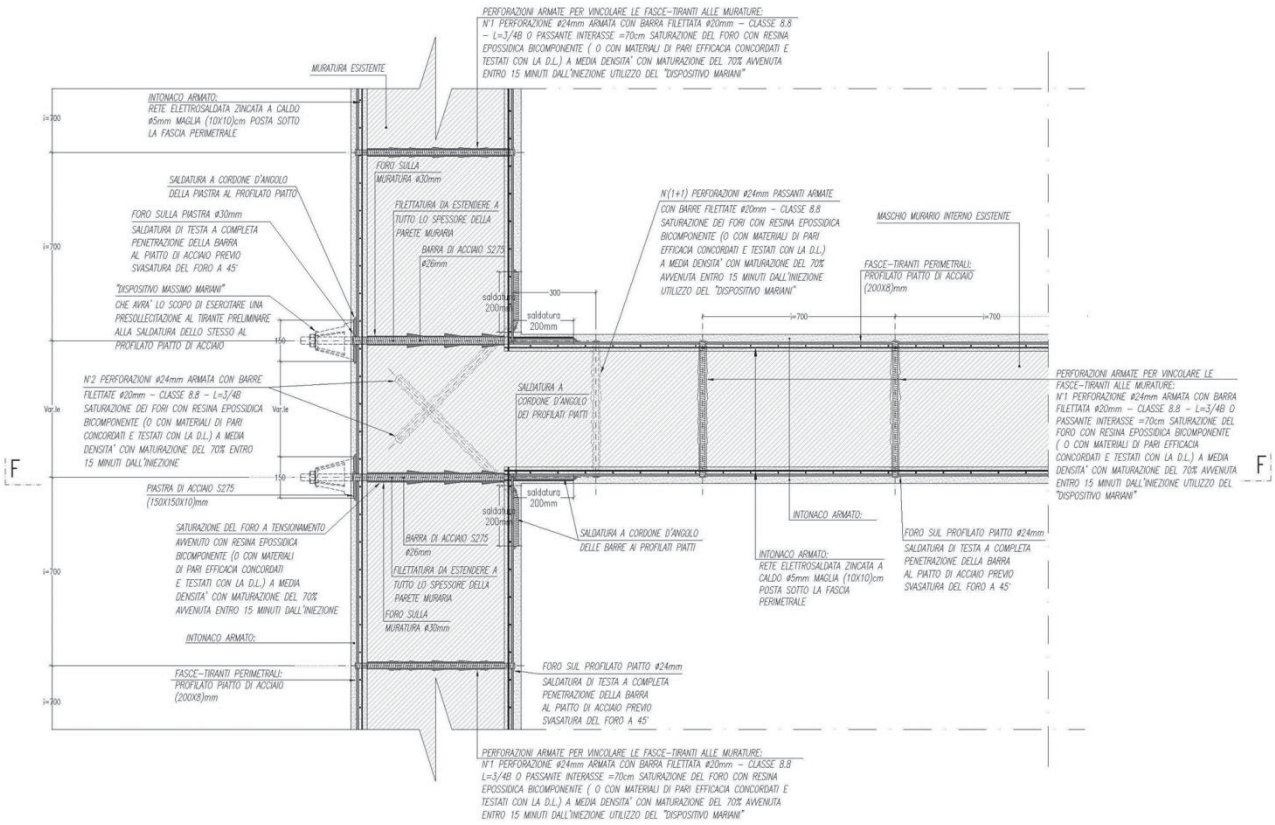

Figure 45. Horizontal connection between orthogonal masonry piers in presence of reinforced mortar on both faces and internal wrapping with steel plates connected to masonry through the "Dispositivo Massimo Mariani", a device allowing to manually prestress the connection jacks in order to enhance the collaboration between steel plate and masonry structure. Prestress is exerted through torque wrench; ties and steel plate are fully covered by the mortar (original drawings by Massimo Mariani)

8 CONCLUSIONS

This work outlined that the variation of acceleration covers an important role in the design of strengthening interventions on existing structures, in particular for masonry buildings. The variation of acceleration is responsible of local failures such as masonry disaggregation and loss of connection between structural elements.

In this context, particularly important is the vertical component of the seismic motion. In that direction the structures feature a non-dissipative behavior and the seismic input may undergo amplification related to resonance phenomena.

As indicated by current technical standards, the seismic evaluation of a structure cannot prescind form an accurate assessment of the local capacities. The latter should always precede analyses that count on the structural dignity of the elements and assess the behavior of the structure as a whole.

This research will be continued by the Authors with the objective of dimensioning the strengthening elements applied in the proposed construction details and providing design solution and analysis methods that take into account the effects of the three-dimensional impulsive actions.

ACKNOWLEDGEMENTS

The authors appreciate the support of colleagues and collaborators that contributed to this research. They would like to thank Luca Ranocchia, Alessia Travanti and Nicola Pero Nullo for the composition and drawing of the construction details; Fulvio Massimo Mariani for the selection of records on ITACA database; Alessio Francioso for the elaborations of Fourier spectra. They also wish to thank Aedes Software for the software Seismic3D developed by Francesco Pugi as part of applied research activities.

REFERENCES

[1] Mariani M.: Terremoto e caos: un nuovo percorso di analisi del comportamento dei sismi, Ingenio, 23.12.2017

[2] Mariani M., Pugi F.: Effetti negativi del sisma verticale sul comportamento delle pareti esistenti in muratura, Ingenio, 25.07.2018

[3] Mariani M., Pugi F., Francioso A.: Sisma verticale: amplificazione della vulnerabilità degli edifici esistenti in muratura, Ingenio, 01.10.2018

[4] Mariani M., Pugi F., Francioso A.: Sisma verticale: modellazione e analisi in ambito professionale sugli edifici esistenti in muratura, Ingenio, 20.12.2018

[5] Mariani M., Pugi F.: Circolare NTC2018: finalmente si dovrà progettare considerando il sisma verticale, Ingenio, 18.02.2019

[6] Mariani M., Pugi F.: Circolare NTC2018: "sisma verticale" da considerare in entrambe le analisi non lineari statica e dinamica, Ingenio, 12.03.2019

[7] Mariani M., Pugi F.: "Sisma verticale" nelle NTC 2018: edifici esistenti e comportamento strutturale "atteso", Ingenio, 03.04.2019

[8] Mariani M., Pugi F., Francioso A.: Vertical component of the seismic action: amplified vulnerability of existing masonry buildings, CompDyn 2019, Crete, Greece, 24–26 June 2019

[9] Mariani M., Pugi F.: La componente sismica verticale è sempre da considerare perché rilevante vicino e lontano dalla sorgente, Ingenio, 07.11.2019

[10] Seismic3D, software, 2020. Sviluppo: F. Pugi, Test: F. Pugi, M. Mariani.

[11] M. Tong, G.-Q. Wang, G.C. Lee: Time derivative of earthquake acceleration, Earthquake Engineering and Engineering Vibration, Vol. 4, No. 1, pp.1-16, June, 2005.

[12] ITACA: ITalian ACcelerometric Archive, http://itaca.mi.ingv.it/ItacaNet_30/#/home

[13] Weihan Weng, Jeffrey Kuo: Jerk decision for free-form surface effects in multi-axis synchronization manufacturing, International Journal of Advanced Manufacturing Technology, 105, pp.799-812, November, 2019.

[14] E.M. Rathje, N.A. Abrahamson, J.D. Bray: Simplified frequency content estimates of earthquake ground motions, J. Geotech. Geoenviron. Eng., 124(2), pp. 150-159, 1998.

[15] Haoxiang He, Ruifeng Li, Kui Chen: Characteristics of Jerk Response Spectra for Elastic and Inelastic Systems, Shock and Vibration, Vol. 2015, Article ID 782748.

[16] Y. Xueshan, Q. Xiaozhai, G.C. Lee, M. Tong, C. Jinming: Jerk and Jerk Sensor, 14th World Conference on Earthquake Engineering, October 12-17, 2008. Beijing, China.

[17] R. Sofronie: Seismic strengthening of masonry in buildings and cultural heritage, SÍSMICA 2004, 6° Congresso Nacional de Sismologia e Engenharia Sísmica, pp.81-100.

[18] R. Sofronie: On the seismic jerk, Journal of Geological Resource and Engineering, Vol. 4, pp.147-152, 2017.

[19] Çelebi, M.: Health monitoring of Buildings Using Threshold Drift Ratios - Now an Established Method, International Conference on Structural Health Monitoring, Vancouver, B.C., Canada, October 2007.

[20] M. Wakui, J. Iyama, T. Koyama: Estimate of plastic deformation of vibrational systems using the high- order time derivative of absolute acceleration, in: Proceedings of the 16th World Conference on Earthquake Engineering, Santiago, 2017.

[21] M. Wakui, J. Iyama: Threshold value and applicable range of nonlinear behavior detection method using second derivative of acceleration, Japan Architectural Review, Vol. 2, No. 2, pp.153-165, April, 2019.

[22] D. Eager, A.M. Pendrill, N. Reistad: Beyond velocity and acceleration: jerk, snap and higher derivatives, European Journal of Physics, 37 (2016) 065008 (11pp).

Historical references about the spatial representation of seismic motion:

[23] B.J. Morrill: *Evidence of record vertical accelerations at Kagel Canyon during the earthquake*, in: The San Fernando, California, earthquake of February 9, 1971, United States Government Printing Office, Washington, 1971.

[24] W.K. Cloud, D.E. Hudson: *A simplified instrument for recording strong-motion earthquakes*, Bulletin of the Seismological Society of America, Vol. 51, No. 2, pp.159-174, April, 1961.

[25] Ronald F. Scott: *The calculation of horizontal accelerations from seismoscope records*, Bulletin of the Seismological Society of America, Vol. 63, No. 5, pp.1637-1661, October, 1973.

[26] C. Arnold, R.Reitherman: *Building configuration and seismic design: the architecture of earthquake resistance*, NSF-CEE 81064, National Science Foundation, Washington, 1981.